

## **Response to Anonymous Referee #2 (Report #1)**

(Note: Reviewer comments are listed in grey, and responses to reviewer comments are in black. Pasted text from the new version of the paper is in italics.)

Dear Editor,

The Authors have addressed most of the questions in an acceptable way and have revised the manuscript accordingly. Still I am not fully convinced about the terms ‘historical urbanization’ or ‘prior to human settlement’. Clearly it is a sensitivity study on the effect of urbanization (roughness elements, excessive heat) on boundary layer structure (dynamical, thermal) which in turn feeds back on chemical reactions and chemical transport processes.

Using identical emissions for different model scenarios further does not relate to a ‘true’ development but highlights more or less an idealized analysis which tries to separate chemical and dynamical effects. A minor point here is, that ‘shrubland’ is not supposed to be the dominant land use from ‘before human settlement’ I think, but more a combination of wetland/grassland/shrubland however. Maybe try to just highlight more prominently that the sensitivity study purely treats the conversion from ‘real’ urban morphology to shrubland for the urban area of LA. In this case I would also recommend to change the term ‘present day’ to ‘Urban’.

We thank the reviewer for the comments and suggestions. Our focus is on land cover changes from “before human settlement” to “present-day”. To make this clear, the abstract states,

*“We assume identical anthropogenic emissions for the simulations carried out, and thus focus on the effect of changes in land surface physical properties and land surface processes on air quality.”*

Shrubland is a reasonable assumption for the dominant land use type for ‘prior to human settlement’ because 1) most of current rural area within Southern California is shrubland, and 2) the major climate types of Southern California include Mediterranean, semi-arid and desert with infrequent rain. The chance of growing a large area of grassland or wetland is low in this region.

Please use the term WRF-Chem instead of WRF/Chem

Thanks for the suggestion. We went through the main paper and supplemental information, and changed all ‘WRF/Chem’ to WRF-Chem.

Compared to your past work, what is the benefit of including the ‘shadow model’

We included the shadow model because it tracks direct and diffuse radiation within the urban canopy separately, whereas with the shadow model turned off, all shortwave radiation within the urban canopy is assumed diffuse. Physically speaking, the first parameterization is more appropriate compared to the second one, thus we turned on the

shadow model. This is discussed already in the last paragraph in section 3.2.3.

*Question 1: The scope of the study...*

Please further highlight your conclusion about the ‘most important land surface factors’

We modified the last paragraph in the conclusion section, and added how the important land surface factors drive changes in regional meteorology and air quality.

*“We find that increases in evapotranspiration, thermal inertia, and surface roughness due to historical urbanization are the main drivers of regional meteorology and air quality changes in Southern California. During the day, our simulations suggest that increases in evapotranspiration and thermal inertia from urbanization lead to regional air temperature reductions. Temperature reductions together with increases in surface roughness contribute to decreases in ventilation and consequent increases in ozone and PM<sub>2.5</sub> concentrations. During nighttime, increases in thermal inertia from urbanization lead to increases in regional air temperatures. Increases in temperatures together with increase in surface roughness lead to decreases in NO<sub>x</sub> and PM<sub>2.5</sub> concentrations. O<sub>3</sub> concentrations increase because of decreased titration by NO<sub>x</sub>.”*

*Question 2: irrigation module*

I still do not get the benefit of using the irrigation module and not discussing the sensitivity on the model results.

The benefit of using the irrigation module is discussed in the last paragraph of section 2.2 in the main paper. Using the irrigation module can improve the model performance in predicting latent heat fluxes and temperatures for the Los Angeles region. In other words, using the irrigation model allows for a more realistic “present-day” scenario. (Please refer to Vahmani and Hogue (2014) for details on the implementation and evaluation of the irrigation module.) Using the irrigation module thus gives us a more reliable result on the effect of land surface changes via urbanization on regional meteorology compared to not involving the irrigation module.

We have also discussed the effect of land surface changes via urbanization without involving irrigation in supplemental information section S3. By comparing the result in section 3.2.1 and 3.2.2 in the main paper with section S3 in supplemental information, we can get the sensitivity of turning on/off irrigation module on the model results. Lastly, a previous paper by our group (Vahmani and Ban-Weiss, 2016a) includes sensitivity simulations with and without irrigation.

Question 3: Past model exercises have shown, that including the multi-layer UCM rather than the single layer model is not per-se a more complex exercise, as it basically just involves changing a switch in the namelist.input. In my understanding, the urban canopy model is further not coupled directly to WRF-Chem but to the (Noah) land-surface model and the link to air chemistry works over the changed atmospheric dynamics. It is correct though, that only a couple of boundary layer schemes do work with BEP and the vertical

levels have to be adapted, but besides the potential higher computational costs, there should not be an enormous amount of extra work. Please comment briefly on that in the revision, or leave out some of the statements.

We agree with the reviewer that the major concern with using BEP is that the resulting model would be potentially more computationally expensive, but for likely little additional benefit in the quality of simulations. Adding the chemistry module already adds immense computational cost. We added a sentence in the first paragraph in section 2.1 to comment on why we used UCM instead of BEP.

*“We used UCM instead of the multilayer canopy layer model (BEP) because BEP would increase computational costs, but for likely little additional benefit in the quality of simulations (Chen et al., 2011; Kusaka et al., 2001).”*

*Question 10: introduction*

How did recent studies make it possible to utilize ‘satellite land surface data’. What is meant by the latter term?

Satellite-retrieved land surface data are those land surface data (e.g., surface albedo, vegetation fraction, leaf area index, etc.) from remote sensing instruments (e.g., MODIS that we used) onboard satellites. Raw satellite-retrieved land surface data cannot be used directly as input in default WRF. Therefore, some recent studies incorporated these data to WRF modeling by adjusting data format and modifying related model code. These studies also assessed the improvements in model performance using land surface data from satellites compared to default data available in the WRF package. Please refer to our previous paper Vahmani and Ban-Weiss, (2016b) as an example of this type of study.

Comment Line 86:

still unclear about the term ‘meteorology can affect emission rates’

Meteorological conditions such as temperature and sunlight intensity can affect rates of biogenic emissions and also evaporative emissions of fuels like gasoline. We added the word ‘biogenic’ to the sentence.

*“Meteorology can affect emission rates (e.g., biogenic volatile organic compounds (BVOCs) and evaporative emissions of gasoline), chemical reaction rates, gas-particle phase partitioning of semi-volatile species, pollutant dispersion, and deposition...”*

Comment to Line 119:

The way, the urban canopy model treats the land surface is not different to other existing studies. The mean values of the various parameters for a grid cell classified as 31,32,33 however are calculated from a potentially higher resolution and state of the art input data set. Maybe I am wrong here, but as you are not considering the tile-approach, the UCM essentially should treat an urban grid cell also as ‘homogenous’. I think it is fair to say something like ‘the urban canopy model is configured for the urban area of Los Angeles, whereas the values in each urban class are calculated including high resolution land

surface/building data'. Not sure though if the impact of this high resolution data set on the final result differs much compared to a more simple urban canopy parametrization and what would be the effect on the difference between Urban-NoUrban.

We are not saying that each urban grid cell has wide heterogeneity, but instead saying that the urban land surface properties for the whole modeling domain shows high spatial heterogeneity. Most past studies use unvarying table-values for land surface properties based on land cover types; thus, properties for any urban cell would be unvarying. We added the word 'spatial' to the related sentence.

*"They also do not resolve the wide spatial heterogeneity of urban land surface properties, with most studies assuming that urban properties are homogenous throughout the city."*

By resolving the real-world spatial heterogeneity in WRF, the model performance of predicting temperature is improved. Our previous research Vahmani and Ban-Weiss (2016b) has shown that using land properties from MODIS reduces model biases in surface and near-surface air temperatures (relative to ground and satellite observations) for urban regions in southern California compared to using default datasets available with WRF. In particular, the root-mean-square-error for nighttime near-surface air temperature has been narrowed from 3.8 to 1.9 °C.

I would recommend to better clarify these points in a revised version in the methodology and discussion/conclusion section.

Ok, please see all responses above.

*Abstract*

Change the term 'before human settlement' here

We think 'before human settlement' is clear to the readers, so we keep the text as it is.

*Underestimation of PM<sub>2.5</sub>:*

The main reason for underestimation of the PM<sub>2.5</sub> concentration in my opinion is the vertical resolution of the model in combination with the problem in comparing point with grid cell. Much of the pollutants measured at the surface might well be diluted by vertical mixing within the first 10s of meters. Can you please present this discussion more clearly, stating further if the particularly poor correlation has the same reasons. I can understand that these systems are not able to picture near surface concentrations, but however you should try to highlight better what are the main points you are interested in (e.g relative differences instead of absolute values).

Thanks to the reviewer for this suggestion. It is a very good point. We added this reason to our explanation of the underestimation of PM<sub>2.5</sub> concentrations, and removed several minor points. We also emphasized that we are interested more in relative differences rather than absolute values. The modified sentences are as follows.

*“The underestimation of  $PM_{2.5}$  concentrations may be occurring mainly due to the following factors: 1) not including dust emissions in the simulation, which makes up an appreciable fraction of real-world total  $PM_{2.5}$ , and 2) while the observations measure values for one single point near the surface, model values represent a grid cell average with a larger spatial “footprint”. Note that the focus of this study is on the changes in pollutant concentrations, and thus relative differences are of increased interest relative to absolute values.”*

## Reference

- Vahmani, P. and Ban-Weiss, G.: Climatic Consequences of Adopting Drought-Tolerant Vegetation Over Los Angeles as a Response to California Drought, *Geophys. Res. Lett.*, 43(15), 8240–8249, 2016a.
- Vahmani, P. and Ban-Weiss, G. A.: Impact of Remotely Sensed Albedo and Vegetation Fraction on Simulation of Urban Climate in WRF-Urban Canopy Model: A Case Study of the Urban Heat Island in Los Angeles, *J. Geophys. Res.-Atmos.*, 121(4), 1511–1531, 2016b.
- Vahmani, P. and Hogue, T. S.: Incorporating an Urban Irrigation Module into the Noah Land Surface Model Coupled with an Urban Canopy Model, *J. Hydrometeorol.*, 15(4), 1440–1456, 2014.

### **Response to Anonymous Referee #3 (Report #2)**

(Note: Reviewer comments are listed in grey, and responses to reviewer comments are in black. Pasted text from the new version of the paper is in italics.)

The revised manuscript is significantly improved compared to the previous version. Many of my comments have been addressed. I have few comments and a concern regarding the interpretation of the statistical significance of the land surface changes impacts on regional meteorology and air quality; and the variable used to derive the confidence levels.

We thank the reviewer for the comments and suggestions. Please find our point-to-point responses as follows.

Major comment:

The authors state in many places of the manuscript “significantly differ from zero at the 95% confidence level” (i.e. line 355, 425, 435, and elsewhere). The measure used for the statistical significance is not meaningful since the differences in the fields simulated under the scenarios considered are likely expected to be different from zero. In fact, even WRF simulations using same configurations but different computer platforms or compiler options can lead to different results due to errors. I would suggest basing the statistical significance on the sign of the difference in the fields simulated. The confidence level at which the difference is positive (negative) if you are expecting increases (decreases) would be more meaningful.

We believe that our current way of carrying out the statistical test is reasonable for the following reasons. Firstly, we used one computing platform and model configuration for all simulations, and thus this cannot be a cause for variability. So if the comparison between two scenarios significantly differs from zero, it is the different settings between these two scenarios that cause the difference. Secondly, different settings between two scenarios does not necessarily mean significant difference in model results if the differences are smaller than model noise. Thus, it is meaningful to check the statistical significance between two model scenarios. Last but not least, this type of statistical test is widely used to study whether changes are significant (Vahmani et al., 2016; Zhang et al., 2016). Using your recommendation to assess significance based only on whether the difference has the same sign as expectation is circular; there is no “expected” sign of change given that many competing pathways contribute to modeled changes. Plus, this would not be an objective approach, only deeming things significant if they follow our expectation.

Other comments:

1- Please indicate the year of the JJA observations discussed in the text (Line 180) and in the caption of Figure S8.

Thanks for catching it. We added ‘year 2012’ in both two places.

2- Line 310: Please use a different word for “validation”. I would suggest “verification”. A complex model like WRF cannot be validated. Verifications of WRF are always required as the WRF results give different results depending on the configurations, regions, periods and the physics parameterizations employed.

Thanks for pointing it out. We changed ‘validation’ to ‘verification’ in the paper and supplemental information.

3- Line 290 and elsewhere: Please reconsider the interpretation of the statistical significance (see the comment above).

Please refer to our response to the major comment.

4- Line 345: I would remove the sentence “Given that the atmosphere is stratified in models”. The discrete approximation shown in Eq2 does not depend on the stratification of the atmosphere since you are not using temperature or density as an independent variable in the integral. I would remove Eq2 (or Eq1) since they are equivalent.

Thanks for the suggestion. We removed Eq1 (since Eq2 is what we actually used to calculate ventilation coefficient) from the paper.

“...*This calculation can be written as (Eq1).*

$$\text{Ventilation Coefficient} = \sum_{i=1}^m U(z_i) \times \Delta z_i \quad (\text{Eq1})$$

where  $U(z_i)$  stands for horizontal wind speed within the  $i^{\text{th}}$  model layer (m/s),  $\Delta z_i$  is the depth of the  $i^{\text{th}}$  model layer that is within the PBL (m), and  $m$  is the number of vertical layers up to PBL height.”

## Reference

- Vahmani, P., Sun, F., Hall, A. and Ban-Weiss, G.: Investigating the Climate Impacts of Urbanization and the Potential for Cool Roofs to Counter Future Climate Change in Southern California, *Environ. Res. Lett.*, 11(12), 124027, 2016.
- Zhang, J., Zhang, K., Liu, J. and Ban-Weiss, G.: Revisiting the climate impacts of cool roofs around the globe using an Earth system model. *Environ. Res. Lett.*, 11(8), 084014, 2016.

# Effects of Urbanization on Regional Meteorology and Air Quality in Southern California

Yun Li<sup>1</sup>, Jiachen Zhang<sup>1</sup>, David J. Sailor<sup>2</sup>, George A. Ban-Weiss<sup>1</sup>

<sup>1</sup>Department of Civil and Environmental Engineering, University of Southern California, Los Angeles, 90007, USA

5 <sup>2</sup>School of Geographical Science and Urban Planning, Arizona State University, Tempe, 85281, USA

Correspondence to: George Ban-Weiss ([banweiss@usc.edu](mailto:banweiss@usc.edu))

## Abstract

Urbanization has a profound influence on regional meteorology and air quality in megapolitan Southern California. The influence of urbanization on meteorology is driven by changes in land surface physical properties and land surface processes. These changes in meteorology in turn influence air quality by changing temperature-dependent chemical reactions and emissions, gas-particle phase partitioning, and ventilation of pollutants. In this study we characterize the influence of land surface changes via historical urbanization from before human settlement to present-day on meteorology and air quality in Southern California using the Weather Research and Forecasting Model coupled to chemistry and the single-layer urban canopy model (~~WRF/Chem~~WRF-UCM-Chem-UCM). We assume identical anthropogenic emissions for the simulations carried out, and thus focus on the effect of changes in land surface physical properties and land surface processes on air quality. Historical urbanization has led to daytime air temperature decreases of up to 1.4 K, and evening temperature increases of up to 1.7 K. Ventilation of air in the LA basin has decreased up to 36.6% during daytime and increased up to 27.0% during nighttime. These changes in meteorology are mainly attributable to higher evaporative fluxes and thermal inertia of soil from irrigation, and increased surface roughness and thermal inertia from buildings. Changes in ventilation drive changes in hourly NO<sub>x</sub> concentrations with increases of up to

10

15

20

2.7 ppb during daytime and decreases of up to 4.7 ppb at night. Hourly O<sub>3</sub> concentrations decrease by up to 0.94 ppb in the morning, and increase by up to 5.6 ppb at other times of day. Changes in O<sub>3</sub> concentrations are driven by the competing effects of changes in ventilation and precursor NO<sub>x</sub> concentrations. PM<sub>2.5</sub> concentrations show slight increases during the day, and decreases of up to 2.5 µg/m<sup>3</sup> at night. Processes drivers for changes in PM<sub>2.5</sub> include modifications to atmospheric ventilation, and temperature, which impacts gas-particle phase partitioning for semi-volatile compounds and chemical reactions. Understanding processes drivers related to how land surface changes effect regional meteorology and air quality is crucial for decision making on urban planning in megapolitan Southern California to achieve regional climate adaptation and air quality improvements.

## 1. Introduction

The world has been undergoing accelerated urbanization since the industrial revolution in the 19<sup>th</sup> Century (Grimm et al., 2008; Seto et al., 2012). Urbanization leads to profound human modification of the land surface and its associated physical properties such as roughness, thermal inertia, and albedo (Fan et al., 2017), and land surface processes like irrigation (Vahmani and Hogue, 2014). These changes in land surface physical properties and processes alter corresponding surface-atmosphere coupling including exchange of water, momentum and energy in urbanized regions (Vahmani and Ban-Weiss, 2016a; Li et al., 2017), which exerts an important influence on regional meteorology and air quality (Vahmani et al., 2016; Civerolo et al., 2007).

Land surface modifications from urbanization drive changes in urban meteorological variables such as temperature, wind speed and planetary boundary layer (PBL) height, which result in urban – rural differences. Differences in surface temperature and near surface air temperature have been widely studied for decades. The urban heat island (UHI) effect, a phenomenon in which temperatures within an

45 urban area are higher than surrounding rural areas (Oke, 1982), has been extensively studied using  
models and observations for a great number of urban regions (Rizwan et al., 2008; Peng et al., 2012;  
Stewart and Oke, 2012). A contrary phenomenon, namely the urban cool island (UCI), under which  
urban temperatures are lower than surrounding rural temperatures, has also been investigated recently in  
some studies (Carnahan and Larson, 1990; Theeuwes et al., 2015; Kumar et al., 2017). Urban – rural  
50 contrast in temperature (i.e. both UHI and UCI) is mainly attributable to differences in thermal  
properties and energy fluxes due to heterogeneous land surface properties. For urban areas, buildings  
and roads (i.e., impervious surfaces) are generally made from manufactured materials (e.g., asphalt  
concrete) with low albedo and thus high solar absorptivity (Wang et al., 2017). These materials also  
have high thermal inertia, which can lead to reductions in diurnal temperature range due to heat storage  
55 and consequent temperature reductions during the day and heat release and consequent temperature  
increases at night (Hardin and Vanos, 2018). Street canyons, which we refer to as the U-shaped region  
between buildings, can trap longwave energy fluxes within the canyon because of reductions of  
sky-view factors (Qiao et al., 2013). On the other hand, shading in street canyons during the day can  
reduce absorption of shortwave radiation (Carnahan and Larson, 1990; Kusaka et al., 2001). Pervious  
60 surfaces within urban areas such as irrigated urban parks and lawns can lead to the urban oasis effect in  
which evaporative cooling occurs due to increases in evapotranspiration. In addition, soil thermal  
properties depend on their water content, which ultimately affects ground heat fluxes and thus surface  
and air temperatures. Land surface properties in surrounding rural areas can also affect urban – rural  
differences in temperature (Imhoff et al., 2010; Peng et al., 2012; Zhao et al., 2014). In particular, urban  
65 regions built in semi-arid or arid surroundings tend to have a weak daytime UHI or even a UCI, whereas  
those built in moist regions tend to have a larger daytime UHI (Fan et al., 2017; Peng et al., 2012).  
Lastly, factors such as anthropogenic heat and atmospheric aerosol burdens can play an important role  
in urban heat/cool island formation in some regions (Oke, 1982; Wang et al., 2017).

Urbanization can also cause differences between urban and rural areas for meteorological variables  
70 other than surface and air temperatures. Changes in regional near-surface wind speed and direction can  
occur in urban areas because of spatially varying modifications in surface roughness (Xu et al., 2006;  
Vahmani et al., 2016). Changes in near surface winds in coastal urban areas can also be affected by  
modifying land-sea temperature contrast (Vahmani et al., 2016). The characteristics of the PBL are  
dependent on the magnitude of turbulent kinetic energy (TKE) (Garratt, 1994). Higher (lower) TKE will  
75 lead to deeper (shallower) PBLs. During daytime, the magnitude of TKE is driven by buoyancy  
production contributed mainly by sensible heat flux (with clear skies); at night, TKE is driven by shear  
production associated with variance in wind speed. Thus, temperature and surface roughness play an  
important role on the depth of the PBL during daytime and nighttime, respectively. Lastly, changes in  
relative humidity, precipitation, and other meteorological variables due to land surface changes can also  
80 be significant in some regions (Burian and Shepherd, 2005; Georgescu et al., 2014).

Changes in meteorological conditions due to urbanization can influence concentrations of air  
pollutants including oxides of nitrogen (NO<sub>x</sub>), ozone (O<sub>3</sub>) and fine particulate matter (PM<sub>2.5</sub>). NO<sub>x</sub> and  
O<sub>3</sub> pollution are major public health concerns in megapolitan regions (Lippmann, 1989). PM<sub>2.5</sub> reduces  
visibility, causes adverse health effects, and alters regional and global climate via direct and indirect  
85 effects (Charlson et al., 1992; Pope and Dockery, 2006; Boucher et al., 2013). Meteorology can affect  
emission rates (e.g., biogenic volatile organic compounds (BVOCs) and evaporative emissions of  
gasoline), chemical reaction rates, gas-particle phase partitioning of semi-volatile species, pollutant  
dispersion, and deposition; thus, it plays an important role in determining air pollutant concentrations.  
Variations in air temperatures together with vegetation types affect the production of ~~biogenic volatile  
90 organic compounds (BVOCs)~~, which are important precursors for ground-level O<sub>3</sub> and secondary  
organic aerosols (SOA) (Guenther et al., 2006). Gas-phase chemical reactions that form secondary

pollutants are also temperature-dependent. Higher (lower) air temperatures in general lead to higher (lower) photolysis reaction rates and atmospheric oxidation rates, which enhance the production of tropospheric O<sub>3</sub>, secondary inorganic aerosols (e.g. nitrate, sulfate, and ammonium aerosols) and SOA (Aw and Kleeman, 2003; Hassan et al., 2013). In addition, concentrations of semi-volatile compounds are affected by equilibrium vapor pressure under various temperature conditions (Pankow, 1997; Ackermann et al., 1998). Higher (lower) temperatures favor phase-partitioning to the gas (particle) phase. Ventilation, which is the combined effect of vertical mixing and horizontal dispersion, can also influence pollutant concentrations (Epstein et al., 2017). Higher (lower) ventilation rates lead to lower (higher) pollutant concentrations especially in coastal cities like Los Angeles where upwind air under typical meteorological conditions is clean relative to urban air. Lastly, changes in surface roughness may affect loss of pollutants via surface deposition, which in turn alters air pollutant concentrations (Abdul-Wahab et al., 2005).

A number of previous studies have investigated the impacts of land surface changes on regional meteorology in a variety of urban regions around the world (Kalnay and Cai, 2003; Burian and Shepherd, 2005; Zhang et al., 2010). However, limited studies have quantified the impact of land surface changes on regional air quality, and most of these studies have focused on changes in surface O<sub>3</sub> concentrations. Civerolo et al. (2007) estimated that land-use changes via urban expansion in New York City can cause increases in near-surface air temperature of 0.6 °C as well as increases in episode-maximum 8h O<sub>3</sub> concentrations of 6 ppb. Jiang et al. (2008) focused on the Houston, Texas area, and found similar relationships between urban expansion, near-surface air temperatures, and O<sub>3</sub>. Nevertheless, only a few studies have included changes in PM<sub>2.5</sub> concentrations. Tao et al. (2015) simulated that spatially averaged surface O<sub>3</sub> concentrations slightly increased (+0.1 ppb) in eastern China due to urbanization, whereas PM<sub>2.5</sub> concentrations decreased by -5.4 µg/m<sup>3</sup> at the near surface.

115 Chen et al. (2018) studied urbanization in Beijing, and found that modification of rural to urban land surfaces has led to increases in near-surface air temperature and PBL height, which in turn led to increases (+9.5 ppb) in surface O<sub>3</sub> concentrations and decreases (−16.6 μg/m<sup>3</sup>) in PM<sub>2.5</sub> concentrations. However, past studies that investigate interactions between land surface changes and changes in meteorology and air quality generally do not identify the major processes driving these interactions. 20 They also do not resolve the wide spatial heterogeneity of urban land surface properties, with most studies assuming that urban properties are homogenous throughout the city. In addition, only few studies investigate interactions between land surface changes and air quality for the Southern California region (Taha, 2015; Epstein et al., 2017; Zhang et al., 2018b), which is one of the most polluted areas in the United States (American Lung Association, 2012).

125 With advances in real-world land surface datasets from satellites, recent modeling studies on land-atmosphere interactions are able to resolve heterogeneous land surface properties and thus better capture urban meteorology, enabling modeling studies that more accurately quantify changes in regional meteorology due to land surface modification. By combining satellite-retrieved high-resolution land surface data with the Weather Research and Forecasting Model coupled to the Single-layer Urban 130 Canopy Model (WRF/UCM), simulations reported in Vahmani and Ban-Weiss (2016a) show improved model performance (i.e. compared to observations) for meteorology in Southern California compared to the default model, which assumes that urban regions have homogeneous urban land cover. A follow-up study, Vahmani et al. (2016), suggested that historical urbanization has altered regional meteorology (e.g., near surface air temperatures and wind flows) in Southern California mainly because of urban 135 irrigation, and changes in land surface thermal properties and roughness. While historical urbanization and its associated impacts on meteorology has the potential to cause important changes in air pollutant concentrations in Southern California, this is never been investigated in past work.

Therefore, this study aims to characterize the influence of land surface changes via historical urbanization on urban meteorology and air quality in Southern California by comparing a “Present-day” scenario with current urban land surface properties and land surface processes to a “Nonurban” scenario assuming land surface distributions prior to human perturbation. To achieve this goal, we adopt a state-of-the-science regional climate-air quality model, the Weather Research and Forecasting Model coupled to chemistry and the Single-layer Urban Canopy Model (~~WRF/Chem~~WRF-UCM-Chem-UCM), and incorporate high-resolution heterogeneity in urban surface properties and processes to predict regional weather and pollutant concentrations. We assess the response of regional meteorology and air quality to individual changes in land surface properties and processes to determine driving factors on atmospheric changes. Note that this paper builds on our prior study Vahmani et al. (2016), but focuses on air quality impacts, whereas our previous research was on meteorological impacts only. While the influence of land surface changes on regional weather has been investigated in numerous past studies, its influence on regional air quality has been seldom studied in past work. In this paper, we aim to quantify the importance of historical land cover change on air pollutant concentrations, and thus the “Nonurban” scenario assumes current anthropogenic pollutant emissions. This hypothetical scenario cannot exist in reality, since current anthropogenic emissions would not exist without the city, but our intent is to tease out the relative importance of land cover change through urbanization (assuming constant emissions) on air pollutant concentrations.

## 2. Methodology and Data

### 2.1 Model Description and Configuration

~~WRF/Chem~~WRF-Chem v3.7 is used in this study to simulate meteorological fields and atmospheric chemistry. ~~WRF/Chem~~WRF-Chem is a state-of-the-science nonhydrostatic mesoscale

160 numerical meteorological model that facilitates “online” simulation of processes relevant to atmospheric chemistry including pollutant emissions, gas and particle phase chemistry, transport and mixing, and deposition (Grell et al., 2005). In this study, we activate the urban canopy model (UCM) in ~~WRF/Chem~~WRF-Chem that resolves land-atmosphere exchange of water, momentum, and energy for impervious surfaces in urban areas (Kusaka et al., 2001; Chen et al., 2011; Yang et al., 2015). The UCM  
165 parameterizes the effects of urban geometry on energy fluxes from urban facets (i.e., roofs, walls, and roads) and wind profiles within canyons (Kusaka et al., 2012). We account for the effect of anthropogenic heat on urban climate by adopting the default diurnal profile in the UCM. We used UCM instead of the multilayer canopy layer model (BEP) because BEP would increase computational costs, but for likely little additional benefit in the quality of simulations (Chen et al., 2011; Kusaka et al.,  
170 2001). Physics schemes included in our model configuration are the Lin cloud microphysics scheme (Lin et al., 1983), the RRTM longwave radiation scheme (Mlawer et al., 1997), the Goddard shortwave radiation scheme (Chou and Suarez, 1999), the YSU boundary layer scheme (Hong et al., 2006), the MM5 similarity surface layer scheme (Dyer and Hicks, 1970; Paulson, 1970), the Grell 3D ensemble cumulus cloud scheme (Grell & Dévényi, 2002), and the unified Noah land surface model (Chen et al.,  
175 2001). Chemistry schemes include the TUV photolysis scheme (Madronich, 1987), RACM-ESRL gas phase chemistry (Kim et al., 2009; Stockwell et al., 1997), and MADE/VBS aerosols scheme (Ackermann et al., 1998; Ahmadov et al., 2012).

All model simulations are carried out from June 28<sup>th</sup>, 2100 UTC (June 28<sup>th</sup>, 1300 PST) to July 8<sup>th</sup>, 0700 UTC (July 7<sup>th</sup>, 2300 PST), 2012 using the North American Regional Reanalysis (NARR) dataset  
180 as initial and boundary meteorological conditions (Mesinger et al., 2006). This simulation period is chosen as representative of typical summer days in Southern California, which are generally clear or mostly sunny without precipitation. A comparison of observed diurnal cycles for average near surface

air temperatures over JJA (June, July and August) in year 2012 versus over our simulation period is shown in Figure S8 in the supplemental information. Hourly model output from July 1<sup>st</sup>, 0000 PST to 7<sup>th</sup>, 2300 PST is used for analysis, and simulation results prior to July 1<sup>st</sup>, 0000 PST are discarded as spin up. Figure 1a shows the three two-way nested domains with horizontal resolutions of 18 km, 6 km and 2 km, respectively, centered at 33.9°N, 118.14°W. Only the innermost domain (141 × 129 grid cells), which encapsulates the Los Angeles and San Diego metropolitan regions, is used for analysis. All three domains consist of 29 unequally spaced layers in the vertical from the ground to 100 hPa. The average depth of the lowest model level is 53 m for all three domains.

## 2.2 Land Surface Property Characterization and Irrigation Parameterization

One important aspect of accurately simulating meteorology and air quality is to properly characterize land surface – atmosphere interactions (Vahmani and Ban-Weiss, 2016a; Li et al., 2017). In addition, accurately quantifying the climate and air quality impacts of historical urbanization requires a realistic portrayal of current land cover in the urban area (Vahmani et al., 2016). For both of these reasons, we update the default ~~WRF/Chem~~ WRF-Chem to include a real-world representation of land surface physical properties and processes.

In this study, we use the (30 m resolution) 33-category National Land Cover Database (NLCD) for the year 2006 for all three model domains. NLCD differentiates three urban types including low-intensity residential, high-intensity residential, and industrial/commercial (shown in Figure 1b) (Fry et al., 2011). In the model (UCM), each of these three types can have unique urban physical properties such as building morphology, albedo, and thermal properties for each facet. We adopt the grid-cell specific National Urban Database and Access Portal Tool (NUDAPT) where available in the innermost domain for building morphology including average building heights, road widths, and roof widths (Ching et al., 2009). Where NUDAPT data are unavailable, we use average building and road

morphology for three urban categories from the Los Angeles Region Imagery Acquisition Consortium (LARIAC). Details on the generation of averaged urban morphology parameters from real-world GIS datasets can be found in Zhang et al. (2018a). For the other parameters in the UCM (e.g., anthropogenic latent heat, surface emissivity), we use default WRF settings documented in file URBPARAM.TBL. Note that the original gaseous dry deposition code based on Wesely (1989) is only compatible with the default 24-category U.S. Geological Survey (USGS) global land cover map. We therefore modify the code according to Fallmann et al. (2016), which assumes that the three urban types in the 33-category system have input resistances that are the same as the urban type for the 24-category system. In addition, impervious fractions (i.e. the fraction of each cell covered by impervious surfaces) for each of the three urban categories in the innermost domain are from the NLCD impervious surface data (Wickham et al., 2013).

Land surface properties including albedo, green vegetation fraction (GVF), and leaf area index (LAI) are important for accurately predicting absorption and reflection of solar radiation and evaporative fluxes in urban areas (Vahmani and Ban-Weiss, 2016a). To resolve high-resolution real-world heterogeneity in these land surface properties, the simulations performed in this study use satellite-retrieved real-time albedo, GVF, and LAI for the innermost domain. Input data compatible with WRF are regridded horizontally using albedo, GVF, and LAI maps generated based on MODIS reflectance (MCD43A4), vegetation indices (MOD13A3), and fraction of photosynthetically active radiation (MCD15A3) products, respectively. Raw data are available from the USGS National Center for Earth Resource Observations and Science website at <http://earthexplorer.usgs.gov>. A detailed description on the implementation of MODIS-retrieved land surface properties for WRF can be found in Vahmani and Ban-Weiss (2016a). Our previous research has shown that the model enhancements described here reduce model biases in surface and near-surface air temperatures (relative to ground and

satellite observations) for urban regions in southern California. In particular, the root-mean-square-error  
230 for nighttime near-surface air temperature has been narrowed from 3.8 to 1.9 °C.

Resolving urban irrigation is also of great significance for accurately predicting latent heat fluxes  
and temperatures within Los Angeles. Here we use an irrigation module developed by Vahmani and  
Hogue (2014), which assumes irrigation occurs three times a week at 2100 PST on the pervious fraction  
of urban grid cells. This model was tuned to match observations of evapotranspiration in the Los  
235 Angeles area. Details on the implementation of this irrigation module and its evaluation with  
observations can be found in Vahmani and Hogue (2014). Note that we do not use the default irrigation  
module available in the single layer canopy model in WRF/UCM v3.7, which assumes daily irrigation  
at 2100 PST in summertime, because (1) the irrigation module of Vahmani and Hogue (2014) was  
already evaluated and tuned for Southern California, and (2) we strive to maintain consistency with our  
240 previous related studies.

## 2.3 Emission Inventories

Producing accurate air quality predictions also relies on using emission inventories that capture  
real-world emissions. We adopt year 2012 anthropogenic emissions from the California Air Resource  
Board (CARB) for the two outer domains (CARB, 2017) where data are available (i.e. within  
245 California), and from South Coast Air Quality Management District (SCAQMD) for the innermost  
domain (SCAQMD, 2017). For areas within the two outer domains that are outside California, we use  
the U.S. Environmental Protection Agency (EPA) National Emissions Inventory (NEI) for 2011 that is  
available with the standard ~~WRF/Chem~~WRF-Chem model (U.S. EPA, 2014). CARB and SCAQMD  
emission inventories as provided have 4 km spatial resolution, with 18 and 11 layers in the vertical from  
250 the ground to 100 hPa, respectively. We regridded these inventories in the horizontal and vertical to  
match the grids of our modeling domains. Note that the aforementioned emission inventories use

chemical speciation from the SAPRC chemical mechanism (Carter, 2003), and thus we have converted species to align with the RACM-ESRL and MADE/VBS mechanisms, both of which use RADM2 (Regional Acid Deposition Model) speciation (Stockwell et al., 1990). The conversion uses species and weighting factors from the emiss\_v04.F script that is distributed with NEI emissions for WRF-Chem modeling. (The original script is available at: <ftp://aftp.fsl.noaa.gov/divisions/taq>.) More details on re-speciating the emissions datasets are presented in the supplemental information (Table S1). For online calculation of biogenic volatile organic emissions we adopt the Model of Emissions of Gases and Aerosols from Nature (MEGAN) (Guenther et al., 2006). The default LAI in MEGAN is substituted with the satellite-retrieved LAI for better quantification of biogenic emissions. Note that we have turned on online calculation of sea salt emissions, but turned off that of dust emissions (both available with default WRF).

## 2.4 Meteorology and Air Pollutant Observations

To facilitate model evaluation, we obtain hourly near-surface air temperature observations, hourly ground-level O<sub>3</sub> and daily PM<sub>2.5</sub> observations within our simulation period. Near-surface air temperature data are gathered from 12 stations from the California Irrigation Management Information System (CIMIS). Air pollutant observations are from the Air Quality System (AQS), which is maintained by the U.S. EPA. Ozone (PM<sub>2.5</sub>) data from 33 (27) air quality monitoring stations are collected representing Los Angeles, Orange, Riverside and San Bernardino Counties. The locations of monitoring stations are shown in Figure S9. Among the 27 monitoring stations where PM<sub>2.5</sub> observations are available, daily PM<sub>2.5</sub> concentrations from gravimetric analysis can be directly obtained from 20 stations, while hourly observations acquired using a Beta Attenuation Monitoring (BAM) are obtained from 15 stations. Hourly PM<sub>2.5</sub> observations at each station are temporally averaged to obtain daily PM<sub>2.5</sub> values.

## 275 2.5 Simulation Scenarios

To investigate the effects of land surface changes via historical urbanization on regional meteorology and air quality in Southern California, we carry out two simulations, which we refer to as the “Present-day” scenario and “Nonurban” scenario. The two scenarios differ only by the assumed land surface properties and processes, which are shown in Figure 2. The Present-day scenario assumes the land cover (Figure 1b) and irrigation of current for Southern California (described in Section 2.2). Urban morphology from NUDAPT and LARIAC, and MODIS-retrieved albedo, GVF and LAI are used in this scenario. To help explain the impact of urbanization without the addition of irrigation, a supplemental simulation, which we refer to as “Present-day No-irrigation”, is also carried out; this simulation is identical to “Present-day” but assumes that there is no irrigation. For the Nonurban scenario, we assume natural land cover prior to human perturbation, and replace all urban grid cells with “shrubs” (Figure 1c). We modify MODIS-retrieved albedo, GVF and LAI in these areas based on properties for shrub lands surrounding urban regions in the Present-day scenario. A detailed explanation on this method (inverse distance weighting approach) can be found in Vahmani et al. (2016). The spatial pattern of land surface properties in both “Present-day” and “Nonurban” scenarios are shown in Figure S10. Note that all three aforementioned scenarios adopt identical anthropogenic emission inventories described in Section 2.3. Using current anthropogenic emissions for “Nonurban” is a hypothetical scenario that cannot exist in reality, but allows us to tease out the effects of land surface changes via urbanization on meteorology and air pollutant concentrations. (Biogenic emissions do change for the scenarios due to changes in land surface properties (e.g., vegetation type and LAI) and meteorology (e.g., temperature).) To check whether the influence on regional meteorology and air quality due to land surface changes are distinguishable from zero, statistical significance at 95% confidence interval is tested using the paired Student’s t-test with  $n = 7$  days

## 2.6 Uncertainties

Note that the results reported in this paper are based on model simulations and are thus dependent on how accurately the regional climate/chemistry model characterizes the climate/chemistry system (e.g., meteorology, surface-atmosphere coupling, and atmospheric chemical reactions). Results may be dependent on model configuration (e.g., physical and chemical schemes), land surface characterizations (e.g., satellite data from MODIS, or default dataset available in WRF) and emission inventories (e.g., anthropogenic emission inventories from CARB, SCAQMD or NEI). In addition, since irrigation is not included in the Nonurban scenario, simulated meteorology in the Nonurban scenario are dependent on assumed soil moisture initial conditions. In this study, we adopt the initial soil moisture conditions from Vahmani et al. (2016) for consistency with our previous work. Soil moisture initial conditions are based on values from six-month simulations without irrigation (Vahmani and Ban-Weiss, 2016b).

## 3. Results and Discussion

### 3.1 Evaluation of Simulated Meteorology and Air Pollutant Concentrations

In this section, we focus on the predicative capability of the model for simulated near-surface air temperature, O<sub>3</sub> and total PM<sub>2.5</sub> concentrations (including sea salt, but excluding dust) for the Present-day scenario. Note that for the evaluation of PM<sub>2.5</sub> concentrations we include only observations from daily (gravimetric) measurements in this section. The comparison between modeled PM<sub>2.5</sub> concentrations versus daily averaged observations derived from hourly BAM measurements is discussed in the supplemental information section S1. In addition, we only include observations from monitoring sites that are located in urban grid cells in the Present-day scenario. The validation verification of near surface air temperatures for both urban and nonurban sites are discussed in section

S2 in the supplemental information. Figure 3 shows the comparison between observed and modeled hourly near surface air temperature, O<sub>3</sub> concentrations, and daily PM<sub>2.5</sub> concentrations. (Comparisons between observed and modeled diurnal cycles for near surface air temperatures and O<sub>3</sub> concentrations are also presented in the supplemental information, Figure S11 and S12.) As shown in Figure 3 (and Figure S11), the model simulations better capture higher air temperatures during the daytime relative to lower values during nighttime. By contrast, predictions of O<sub>3</sub> and PM<sub>2.5</sub> concentrations show good fit with observations at low values that occur with high occurrence frequency. However, observed O<sub>3</sub> and PM<sub>2.5</sub> concentrations are underestimated by the model at higher values that occur with lower frequency of occurrence. The underestimation of PM<sub>2.5</sub> concentrations may be occurring mainly due to ~~one or more of~~ the following factors: 1) not including dust emissions in the simulation, which makes up an appreciable fraction of real-world total PM<sub>2.5</sub>, and 2) while the observations measure values for a single point near the surface, model values represent a grid cell average with a larger spatial “footprint”. Note that the focus of this study is on the changes in pollutant concentrations, and thus relative differences are of increased interest relative to absolute values. ~~2) a failure of the emissions inventory to capture high emission rates on particular days, 3) the chemistry parameterizations in WRF/Chem tending to underestimate PM<sub>2.5</sub> concentrations at high values, and 4) errors in simulated air pollution meteorology.~~ Table 1 shows four statistical metrics for model evaluation, including mean bias (MB) and normalized mean bias (NMB) for the quantification of bias, and mean error (ME) and root mean square error (RMSE) for the quantification of error. The statistical results indicate that model simulations underestimate near-surface air temperature, O<sub>3</sub> and PM<sub>2.5</sub> concentrations by 1.0 K, 22% and 31%, respectively. The comparison between our evaluation results and recommended model performance benchmarks is presented in the supplemental information Table S2.

## 3.2 Effects of Urbanization on Air Temperature and Ventilation Coefficient

The effects of land surface changes via urbanization in Southern California on air temperature and ventilation coefficient are discussed in this section. Air temperatures are reported for the lowest atmosphere model layer rather than the default diagnostic 2m (near-surface) air temperature variable to be consistent with reported air pollutant concentrations shown in later sections. (The chemistry code makes use of grid cell air temperature and does not use 2m air temperature.) Ventilation coefficient is calculated as the product of PBL height and the average wind speed within the PBL, and thus considers the combined effects of vertical and horizontal mixing, and indicates the ability of the atmosphere to disperse air pollutants (Ashrafi et al., 2009). ~~The integral form of t~~This calculation can be written as (Eq1).

$$\text{Ventilation Coefficient} = \int_0^{\text{PBL height}} U(z) dz \quad (\text{Eq1})$$

~~Given that the atmosphere is stratified in models, Eq1 can be discretized as Eq2:~~

$$\text{Ventilation Coefficient} = \sum_{i=1}^m U(z_i) \times \Delta z_i \quad (\text{Eq12})$$

where  $U(z_i)$  stands for horizontal wind speed within the  $i^{\text{th}}$  model layer (m/s),  $\Delta z_i$  is the depth of the  $i^{\text{th}}$  model layer that is within the PBL (m), and  $m$  is the number of vertical layers up to PBL height.

### 3.2.1 Spatial average temperature change

As shown in Figure 4a, urbanization in Southern California has in general led to urban temperature reductions during daytime from 7 PST to 16 PST, and urban temperature increases during other times of day. The largest spatially averaged temperature reduction occurs at 10 PST ( $\Delta T = -1.4$  K), whereas the largest temperature increase occurs at 20 PST (+1.7 K). Additionally, urbanization led to spatially averaged reduction in diurnal temperature range by 1.5 K. Spatially averaged urban temperature

reductions during morning (i.e., defined here and in the following sections as 7:00 – 12:00 PST) and afternoon (i.e., 12:00 – 19:00 PST) are  $-0.9$  K and  $-0.3$  K, respectively. At nighttime (i.e., 19:00 – 7:00 PST), the spatially averaged temperature increase is  $+1.1$  K. The spatially averaged changes significantly differ from zero at the 95% confidence level for all three times of the day using the paired Student's t-test with  $n=7$  days.

### 3.2.2 Spatial distributions of temperature change

During the morning, temperature reductions are larger in regions further away from the sea (e.g., San Fernando Valley and Riverside County) than coastal regions (e.g., west Los Angeles and Orange County) (Figure 5a). (Note that regions that are frequently mentioned in this study are in Figure 2a.) Spatial patterns in the afternoon are similar to morning, with the exception that coastal regions experience temperature increases (as opposed to decreases) of up to  $+0.82$  K (Figure 5b). During nighttime, temperature increases spread throughout urban regions, and are generally larger in the inland regions of the basin relative to coastal regions (Figure 5c). A modified version Figure 5 that includes values for non-urban cells is in the supplemental information Figure S13.

### 3.2.3 Processes driving daytime changes

The temporal and spatial patterns of air temperature changes suggest that the climate response to urbanization during daytime is mainly associated with the competition between (a) temperature reductions from increased evapotranspiration and thermal inertia from urban irrigation, and (b) temperature increases from decreased onshore sea breezes (Figure S14d, e). Decreases in the onshore sea breeze are primarily caused by increased roughness lengths from urbanization. (Note that the onshore sea breeze decreases in strength despite higher temperatures in the coastal region of Los Angeles during the afternoon, which would tend to increase the land-sea temperature contrast and thus

be expected to increase the sea breeze strength.) Inland regions show larger temperature reductions  
385 relative to coastal because they have lower urban fractions (Figure S10a), and thus higher pervious  
fractions. Since irrigation increases soil moisture in the pervious fraction of the grid cell in this model,  
irrigation will have a larger influence on grid cell averaged latent heat fluxes (Figure S15) and thermal  
inertia when pervious fractions are higher. The inland regions are also less affected by changes in the  
sea breeze relative to coastal regions since they are (a) farther from the ocean, and (b) experience  
390 smaller increases in roughness length. Roughness length effects on the sea breeze are especially  
important in the afternoon when baseline wind speeds are generally highest in the Los Angeles basin.  
Thus, the afternoon temperature increases simulated in the coastal region occur because temperature  
increases from reductions in the afternoon onshore flows dominate over temperature decreases from  
increased evapotranspiration. In addition, increases in thermal inertia caused by use of manmade  
395 materials (e.g., pavements and buildings) can contribute to simulated temperature reductions during the  
morning. Please see the supplemental information section S3 for the additional simulation (Present-day  
No-irrigation scenario) carried out to identify the influence of urbanization but without changing  
irrigation relative to the Nonurban scenario (i.e., with no irrigation).

Note that changes in air temperature during daytime shown here disagree with Vahmani et al.  
400 (2016). While our study detects daytime temperature reductions due to urbanization, Vahmani et al.  
(2016) suggests daytime warming. After detailed comparison of the simulations in our study versus  
Vahmani et al. (2016), we find that the differences are mainly associated with UCM configuration. First,  
our study uses model default calculations of surface temperature for the impervious portion of urban  
grid cells, whereas Vahmani et al. (2016) applied an alternative calculation proposed by Li and  
405 Bou-Zeid, 2014. Li and Bou-Zeid, 2014 intended the alternate surface temperature calculations to be  
performed as a post-processing step rather than during runtime. After a careful comparison among

different model set-ups, we found that the parameterization of surface temperature is an important factor that affects simulated daytime air temperature (See Figure S16). Second, our study accounts for shadow effects in urban canopies, whereas Vahmani et al. (2016) assumes no shadow effects. (We note here that the default version of the UCM has the shadow model turned off. The boolean SHADOW variable in module\_sf\_urban.F needs to be manually switched to true to enable the shadow model calculations. With the shadow model turned off, all shortwave radiation within the urban canopy is assumed diffuse.) We suggest that it is important to include the effects of building morphology on shadows within the canopy, and to track direct and diffuse radiation separately, and therefore perform simulations in this study with the shadow model on. Note that the effect of shadows is not as significant as the parameterization of surface temperature for most of the domain in our study because the ratio between building height and road width is small.

### **3.2.4 Processes driving nighttime changes**

The climate response to urbanization during nighttime is driven by the combined effects of (a) temperature increases from increasing upward ground heat fluxes, and (b) temperature increases from increasing PBL heights. Increased soil moisture (from irrigation) and use of man-made materials leads to higher thermal inertia of the ground; this in turn leads to increased heat storage during the day and higher upward ground heat fluxes and thus surface temperatures at night. Increasing PBL heights can also lead to warming because of lower air cooling rates during nighttime. Changes in PBL heights are associated with surface roughness changes since shear production dominates TKE at night. Coastal (inland) regions show larger (smaller) variation in roughness length (Figure 2e), which leads to larger (smaller) increases in PBL heights (Figure S14c). Despite larger increases in PBL heights in coastal versus inland regions, smaller air temperature increases occur in coastal versus inland regions, likely due to accumulative effects from coastal to inland regions with onshore wind flows.

### 430 3.2.5 Temporal and spatial patterns of ventilation changes and process drivers

Changes in ventilation coefficient show a similar temporal pattern as air temperature (Figure 4b); values decrease by up to  $-36.6\%$  (equivalent to  $-826 \text{ m}^2/\text{s}$ , at 10 PST) during daytime, and increase up to  $+27.0\%$  (equivalent to  $+77 \text{ m}^2/\text{s}$ , at 23 PST) during nighttime, due to urbanization. Absolute reductions in ventilation coefficient are more noticeable in the afternoon than in the morning; the  
435 spatially averaged decreases are  $-726 \text{ m}^2/\text{s}$  ( $-23\%$ ) and  $-560 \text{ m}^2/\text{s}$  ( $-34\%$ ), respectively. These reductions significantly differ from zero at 95% confidence level using the paired Student's t-test with  $n=7$  days. Reductions during daytime are also generally greater in inland regions than in coastal regions as shown in Figure 5d and 5e. Daytime reductions in ventilation occur due to the combined effect of  
440 weakened wind speeds due to higher surface roughness and changes (mostly decreases) in PBL heights (Figure S14). Changes in PBL heights during daytime are mainly associated with air temperature changes because buoyancy production dominates TKE during the day. Where there are larger air temperature decreases (increases), there is reduced (increased) buoyancy production of TKE, which results in shallower (deeper) PBLs.

At night, spatially averaged ventilation coefficient increases by  $+8.2\%$  ( $+24.3 \text{ m}^2/\text{s}$ ). This increase  
445 significantly differs from zero at 95% confidence level. As shown in Figure 5f, statistically significant ventilation growth occurs in most parts of coastal Los Angeles and Orange County, likely due to higher PBL height increases (i.e., stemming from higher surface roughness increases from urbanization). By contrast, in Riverside County, the effect of reductions in wind speed surpasses changes in PBL heights, leading to slight but not statistically significant reductions in atmospheric ventilation (Figure S14).

### 450 **3.3 Effects of Urbanization on NO<sub>x</sub> and O<sub>3</sub> Concentrations due to Meteorological Changes**

Concentrations of pollutants are profoundly impacted by meteorological conditions including air temperature and the ventilation capability of the atmosphere (Aw and Kleeman, 2003; Rao et al., 2003). This section discusses how meteorological changes due to land surface changes via urbanization in 455 Southern California affect gaseous pollutant concentrations (i.e., NO<sub>x</sub> and O<sub>3</sub>).

#### **3.3.1 Temporal and spatial patterns of NO<sub>x</sub> concentration changes and process drivers**

As shown in Figure 6a, changes in meteorological fields due to urbanization have led to increases in hourly NO<sub>x</sub> concentrations during the day (7 PST to 18 PST) and decreases at all other times of day. Peak increases in NO<sub>x</sub> of +2.7 ppb occur at 10 PST (i.e., for spatial mean values), while peak decreases 460 of -4.7 ppb occur at 21 PST. Spatial mean changes in NO<sub>x</sub> concentrations are +2.1 ppb and +1.2 ppb in the morning and afternoon, respectively, and -2.8 ppb at night. The spatially averaged changes are significantly different from zero at 95% confidence level for all three times of the day. In addition, daily 1-hour maximum NO<sub>x</sub> concentrations change only slightly: from 17.8 ppb at 6 PST in the Nonurban scenario to 17.9 ppb at 7 PST in the Present-day scenario.

465 Figures 7a,b,c show the spatial patterns of NO<sub>x</sub> concentration changes due to urbanization. In the morning (afternoon), most inland urban regions show statistically significant increases in NO<sub>x</sub> concentrations (Figure 7a, b), with larger NO<sub>x</sub> concentration increases of up to +13.8 ppb (+5.5 ppb) occurring in inland regions compared to coastal regions. By contrast, NO<sub>x</sub> concentrations decrease at night across the region, with the largest decreases reaching -20.8 ppb. In general, greater decreases are 470 shown in inland regions compared to coastal regions.

The spatial patterns of changes in NO<sub>x</sub> concentrations are similar to those for CO concentrations

(Figure 7d,e,f). CO is an inert species and can be used as a tracer for determining the effect of ventilation on air pollutant dispersion since it includes accumulation effects of ventilation changes both spatially and temporally. Thus, the similarity in changes to NO<sub>x</sub> and CO spatial patterns suggests that NO<sub>x</sub> changes are driven by ventilation changes. For example, at night, Riverside County shows decreases of up to -20.8 ppb in NO<sub>x</sub> concentrations (with corresponding decreases in CO of -119 ppb) despite suppressed ventilation at this location because of accumulative effects from coastal to inland regions. A modified version of Figure 7 that includes values for non-urban cells is in the supplemental information Figure S17.

### 3.3.2 Temporal and spatial patterns of O<sub>3</sub> concentration changes

As indicated by Figure 6b, O<sub>3</sub> concentrations in the lowest atmospheric layer decrease from 7 PST to 11 PST, and increase during other times of day. The largest decrease of -0.94 ppb occurs at 10 PST, while the largest increase of +5.6 ppb occurs at 19 PST. Spatially averaged hourly O<sub>3</sub> concentrations undergo a -0.6 ppb decrease, +1.7 ppb increase, and +2.1 ppb increase in the morning, afternoon, and night, respectively. The spatially averaged changes significantly differ from zero at 95% confidence level for all three times of the day. Additionally, daily 1-hour maximum O<sub>3</sub> concentrations, which occurs at 14 PST in both scenarios, increases by +3.4%, from 41.3 ppb in the Nonurban scenario to 42.7 ppb in the Present-day scenario. The daily 8-hour maximum O<sub>3</sub> concentration increases from 38.0 ppb to 39.3 ppb (averaged over 11 PST to 19 PST in both scenarios).

Figure 7g,h,i show the spatial patterns of surface O<sub>3</sub> concentration changes. In the morning (Figure 7g), while most regions show reductions in O<sub>3</sub> concentrations, the reductions are in general statistically insignificant. During the afternoon, most inland urban regions show increases in O<sub>3</sub> concentrations (Figure 7h), with the largest increase of +5.7 ppb occurring in Riverside County. Increases in O<sub>3</sub> concentrations are larger during night than the afternoon (Figure 7i), especially in the Riverside County,

495 with the largest increase in O<sub>3</sub> concentrations reaching +12.8 ppb.

### 3.3.3 Processes driving daytime and nighttime changes in O<sub>3</sub>

The temporal and spatial patterns of changes in O<sub>3</sub> concentrations during the day suggest that these changes are mainly driven by the competition between (a) decreases in ventilation, which would tend to cause increases in O<sub>3</sub>, and (b) the nonlinear response of O<sub>3</sub> to NO<sub>x</sub> changes. In the VOC-limited regime, increases in NO<sub>x</sub> tend to decrease O<sub>3</sub> concentrations, and vice versa. (This explains why decreases in NO<sub>x</sub> emissions over weekends can cause increases in O<sub>3</sub> concentrations, a phenomenon termed the “weekend effect” (Marr & Harley, 2002).) The underlying cause of the weekend effect has to do with titration of O<sub>3</sub> by NO, as shown in R1.



505 When NO<sub>x</sub> is high relative to VOC, R1 dominates NO to NO<sub>2</sub> conversion, which involves consuming O<sub>3</sub>. In addition, increases in NO<sub>2</sub> can reduce OH lifetime due to increased rates of the OH + NO<sub>2</sub> reaction (R2), which is chain terminating.



In addition to these two aforementioned processes, changes in air temperature can also affect the production rate of O<sub>3</sub>, with higher temperatures generally leading to higher O<sub>3</sub> (Steiner et al., 2010).

In the morning when ventilation is relatively weak (shallow PBL and weak sea breeze), changes in NO<sub>x</sub> concentrations play an important role in driving surface O<sub>3</sub> concentrations. Regions with greater increases in NO<sub>x</sub> concentrations in general show greater decreases in O<sub>3</sub> concentrations (Figure 7g). Decreases in air temperature would also contribute to decreases in O<sub>3</sub> concentrations due to reductions in O<sub>3</sub> production rates. In the afternoon when ventilation is strengthened (deep PBL, and stronger sea

breeze), changes in both NO<sub>x</sub> concentrations and ventilation play important roles in determining O<sub>3</sub> concentrations (Figure 7h). Regions with higher increases in NO<sub>x</sub> concentrations tend to have lower increases in O<sub>3</sub> concentrations; this indicates that NO<sub>x</sub> increases (that would tend to decrease O<sub>3</sub>) are counteracting decreases in ventilation (that would tend to increase O<sub>3</sub>). In regions with relatively lower increases in NO<sub>x</sub> concentrations and greater decreases in ventilation, such as Riverside County, increases in O<sub>3</sub> concentrations are larger.

At night, changes in O<sub>3</sub> concentrations are dominated by its titration by NO<sub>2</sub> as shown in (R3).



Where there are larger decreases in NO<sub>x</sub> concentrations (Figure 7c), there are greater increases in O<sub>3</sub> concentrations (Figure 7i), regardless of the magnitude of increases in atmospheric dilution (Figure 5f).

### **3.4 Effects of Urbanization on Total and Speciated PM<sub>2.5</sub> Concentrations due to Meteorological Changes**

In this section, we discuss changes in total and speciated PM<sub>2.5</sub> mass concentrations due to urbanization. Total mass concentrations reported here only consider PM<sub>2.5</sub> generated from anthropogenic and biogenic sources mentioned in section 2.3, and exclude sea salt and dust. Speciated PM<sub>2.5</sub> is classified into three categories: (secondary) inorganic aerosols including nitrate (NO<sub>3</sub><sup>-</sup>), sulfate (SO<sub>4</sub><sup>2-</sup>) and ammonium (NH<sub>4</sub><sup>+</sup>); primary carbonaceous aerosols including elemental carbon (EC), and primary organic carbon (POC); and secondary organic aerosol (SOA) including SOA formed from anthropogenic VOC precursors (ASOA) and biogenic VOC precursors (BSOA).

#### **3.4.1 Temporal patterns of total and speciated PM<sub>2.5</sub> concentration changes**

Figure 8 illustrates diurnal changes in total and speciated PM<sub>2.5</sub> concentrations due to

meteorological changes attributable to urbanization. As suggested by Figure 8a, urbanization is simulated to cause slight spatially averaged increases in total PM<sub>2.5</sub> concentrations from 9 PST to 16 PST (up to +0.62 μg/m<sup>3</sup> occurring at 12 PST), and decreases during other times of day (up to -3.1 μg/m<sup>3</sup> at 0 PST). Increases in total PM<sub>2.5</sub> during 9 PST to 16 PST come from increases in primary carbonaceous aerosols, and nitrate; these species show hourly averaged concentration increases of up to +0.21, +0.14 μg/m<sup>3</sup>, respectively. By contrast, BSOA decreases slightly during these hours. During other times of day, concentrations of all PM<sub>2.5</sub> species decrease dramatically. Inorganic aerosols, primary carbonaceous aerosols, and SOA show decreases of up to -1.7, -0.5 and -0.3 μg/m<sup>3</sup>, respectively.

During morning hours, averaged hourly total PM<sub>2.5</sub> concentrations decrease by -0.20 μg/m<sup>3</sup> but are not statistically significant. In the afternoon, spatially averaged total PM<sub>2.5</sub> concentrations increase by +0.24 μg/m<sup>3</sup>. Primary carbonaceous aerosols contribute to half of the increase (+0.12 μg/m<sup>3</sup>). For nighttime, total PM<sub>2.5</sub> concentrations undergo a decrease of -2.5 μg/m<sup>3</sup>, with 54% of the decrease attributed to changes in inorganic aerosols and 17% by primary carbonaceous aerosols. Both afternoon and nighttime changes are significantly different from zero at 95% confidence interval.

### 3.4.2 Spatial patterns of total and speciated PM<sub>2.5</sub> concentration changes

Figure 9 presents spatial patterns of changes in total and speciated PM<sub>2.5</sub> due to urbanization. Decreases in concentrations prevail in urban regions during morning and night, whereas increases in concentrations are dominant during the afternoon.

In the morning, changes in total PM<sub>2.5</sub> and speciated PM<sub>2.5</sub> are not statistically distinguishable from zero at 95% confidence level. In the afternoon, increases in total PM<sub>2.5</sub> are statistically significant in only some inland regions, driven mostly by increases in primary carbonaceous aerosols (up to +0.5 μg/m<sup>3</sup>).

g/m<sup>3</sup>, Figure 9h). At night, most regions within the Los Angeles metropolitan area show decreases in  
560 total PM<sub>2.5</sub> of -3.0 to -6.0 μg/m<sup>3</sup> (Figure 9c) with contributions from all three categories of speciated  
PM<sub>2.5</sub>.

A modified version of Figure 9 that includes values for non-urban cells is in the supplemental  
information Figure S18.

### 3.4.3 Processes driving daytime and nighttime changes in PM<sub>2.5</sub>

565 During the day, changes in speciated PM<sub>2.5</sub> concentrations are dictated by the relative importance of  
various competing pathways, including (a) reductions in ventilation causing increases in PM<sub>2.5</sub>, (b)  
changes in gas-particle phase partitioning causing increases (decreases) in PM<sub>2.5</sub> from decreases  
(increases) in temperature, and (c) increases (decreases) in atmospheric oxidation from increases  
(decreases) in temperature. Changes in ventilation appear to dominate the changes in primary  
570 carbonaceous aerosols, as indicated by the similarity in spatial pattern to changes in CO, which can be  
considered a conservative tracer (Figure 7d and 7e). As for semi-volatile compounds such as nitrate  
aerosols (red dotted curve in Figure 8b) and some SOA species, concentrations increase during daytime  
hours. This is because both decreased ventilation and gas-particle phase partitioning effects favoring the  
particle phase (from temperature decreases) outweigh reductions in atmospheric oxidation.  
575 Concentrations of sulfate and ammonium slightly increase due to urbanization (blue dotted curve in  
Figure 8b). Since sulfate is nonvolatile, gas-particle phase partitioning does not affect sulfate  
concentrations; lowered atmospheric oxidation rates due to reduced temperatures (which would tend to  
decrease sulfate) nearly offset the effect of weakened ventilation (which would tend to increase sulfate).  
In addition, BSOA concentrations are simulated to decrease (blue dotted curve in Figure 8d) due to  
580 reduced biogenic VOC emissions, which occur due to reductions in both vegetation coverage and air  
temperature from urbanization.

At night, decreases in PM<sub>2.5</sub> across urban regions are due to (1) enhanced ventilation owing to deeper PBLs (relevant for all PM species), and (2) gas-particle phase partitioning effects that favor the gas phase for semi-volatile compounds (i.e., nitrate aerosols and some SOA species) because of higher  
585 air temperatures.

## 4. Conclusion

In this study, we have characterized the impact of land surface changes via urbanization on regional meteorology and air quality in Southern California using an enhanced version of ~~WRF/Chem~~WRF-UCM-Chem-UCM. We use satellite data for the characterization of land surface properties, and include a Southern California-specific irrigation parameterization. The two main  
590 simulations of focus in this study are the real-world “Present-day” and the hypothetical “Nonurban” scenarios; the former assumes current land cover distributions and irrigation of vegetative areas, while the latter assumes land cover distributions prior to widespread urbanization and no irrigation. We assume identical anthropogenic emissions in these two simulations to allow for focusing on the effects  
595 of land cover change on air pollutant concentrations.

Our results indicate that land surface modifications from historical urbanization have had a profound influence on regional meteorology. Urbanization has led to daytime reductions in air temperature for the lowest model layer and reductions in ventilation within urban areas. The impact of urbanization at nighttime shows the opposite effect, with air temperatures and ventilation coefficients  
600 increasing. Spatially averaged reductions in air temperature and ventilation during the day are  $-0.6$  K and  $-650$  m<sup>2</sup>/s respectively, whereas increases at night are  $+1.1$  K and  $24.3$  m<sup>2</sup>/s respectively. Changes in meteorology are spatially heterogeneous; greater changes are simulated in inland regions for (a) air temperatures decreases during day and increases during night, and (b) ventilation reductions during

605 daytime. Ventilation at night shows increases in coastal areas and decreases in inland areas. Changes in meteorology are mainly attributable to (a) increased surface roughness from buildings, (b) higher evaporative fluxes from irrigation, and (c) higher thermal inertia from building materials and increased soil moisture (from irrigation).

Changes in regional meteorology in turn affect concentrations of gaseous and particulate pollutants. NO<sub>x</sub> concentrations in the lowest model layer increase by +1.6 ppb during the day, and decrease by – 610 2.8 ppb at night, due to changes in atmospheric ventilation. O<sub>3</sub> concentrations decrease by –0.6 ppb in the morning, and increase by +1.7 (2.2) ppb in the afternoon (night). Decreases in the morning and increases during other times of day are more noticeable in inland regions. Changes in O<sub>3</sub> concentrations are mainly attributable to the competition between (a) changes in atmospheric ventilation, and (b) changes in NO<sub>x</sub> concentrations that alter O<sub>3</sub> titration. Note that while changes in air temperature can 615 also influence O<sub>3</sub> concentrations during the day, this effect is overwhelmed by changes in ventilation and concentrations of NO<sub>x</sub> in our study. As for PM<sub>2.5</sub>, total mass concentrations increase by +0.24 μg/m<sup>3</sup> in the afternoon, and decrease by –2.5 μg/m<sup>3</sup> at night. Changes during the morning are not statistically significant. The major driving processes of changes in PM<sub>2.5</sub> concentrations are (a) changes in atmospheric ventilation, (b) changes in gas-particle phase partitioning for semi-volatile compounds 620 due to air temperature changes, and (c) changes in atmospheric chemical reaction rates from air temperature changes.

This study highlights the role that land cover properties can have on regional meteorology and air quality. We find that increases in evapotranspiration, thermal inertia, and surface roughness due to historical urbanization are the main drivers of regional meteorology and air quality changes in Southern 625 California. During the day, our simulations suggest that increases in evapotranspiration and thermal inertial from urbanization ~~has lead~~ to regional air temperature reductions. ~~but~~ Temperature reductions

630 together with increases in surface roughness contribute to decreases in ventilation and consequent  
increases in ozone and PM<sub>2.5</sub> concentrations. During nighttime, increases in thermal inertial from  
urbanization ~~has lead~~ to increases in regional air temperatures, ~~and O<sub>3</sub> concentrations, but~~ Increases in  
635 temperatures together with increase in surface roughness lead to decreases in NO<sub>x</sub> and PM<sub>2.5</sub>  
concentrations. O<sub>3</sub> concentrations increase because of decreased titration by NO<sub>x</sub>. Our findings indicate  
that air pollutant concentrations have been impacted by land cover changes since pre-settlement times  
(i.e., urbanization), even assuming constant anthropogenic emissions. These air pollutant changes are  
driven by urbanization-induced changes in meteorology. This suggests that policies that impact land  
635 surface properties (e.g., urban heat mitigations strategies) can have impacts on air pollutant  
concentrations (in addition to meteorological impacts); to the extent possible, all environmental systems  
should be taken into account when studying the benefits or potential penalties of policies that impact the  
land surface in cities.

## Author Contributions

640 GBW designed the study. YL performed the model simulations, carried out data analysis, and wrote  
the manuscript. GBW and DS mentored YL. JZ contributed to the setup of  
~~WRF/Chem~~ WRF-UCM-Chem-UCM. All authors contributed to editing the paper.

## Competing Interests

The authors declare that they have no conflict of interest.

## 645 **Acknowledgements**

This research is supported by the US National Science Foundation under grants CBET-1512429, CBET-1623948, and grant CBET-1752522. Model simulations for the work described in this paper are supported by the University of Southern California's Center for High-Performance Computing (<https://hpcc.usc.edu/>). We thank Scott Epstein and Sang-Mi Lee at South Coast Air Quality  
650 Management District, Jeremy Avise at California Air Resources Board for providing us emission datasets. We also thank Ravan Ahmadov and Stu McKeen at National Oceanic and Atmospheric Administration for their helpful suggestions.

## **Reference**

- 655 Abdul-Wahab, S. A., Bakheit, C. S., and Al-Alawi, S. M.: Principal component and multiple regression analysis in modelling of ground-level ozone and factors affecting its concentrations, *Environ. Modell. Softw.*, 20(10), 1263–1271, 2005.
- Ackermann, I. J., Hass, H., Memmesheimer, M., Ebel, A., Binkowski, F. S., and Shankar, U.: Modal aerosol dynamics model for Europe: development and first applications, *Atmos. Environ.*, 32(17), 2981–2999, 1998.
- 660 Ahmadov, R., McKeen, S. A., Robinson, A. L., Bahreini, R., Middlebrook, A. M., de Gouw, J. A., Meagher, J., Hsie, E.-Y., Edgerton, E., Shaw, S., and Trainer, M.: A volatility basis set model for summertime secondary organic aerosols over the eastern United States in 2006, *J. Geophys. Res.-Atmos.*, 117, D06301, 2012.
- American Lung Association: State of the Air 2012, available at:  
665 <http://www.stateoftheair.org/2012/assets/state-of-the-air2012.pdf>, 2012.
- Ashrafi, K., Shafie-Pour, and Kamalan, H.: Estimating Temporal and Seasonal Variation of Ventilation Coefficients, *Int. J. Environ. Res.*, 3(4), 637–644, 2009.
- Aw, J., and Kleeman, M. J.: Evaluating the first-order effect of intraannual temperature variability on urban air pollution, *J. Geophys. Res.*, 108(D12), 4365, 2003.

- 670 Boucher, O., Randall, D., Artaxo, P., Bretherton, C., Feingold, G., Forster, P., Kerminen, V.-M., Kondo, Y., Liao, H., Lohmann, U., Rasch, P., Satheesh, S. K., Sherwood, S., Stevens, B. and Zhang, X. Y.: Clouds and Aerosols, in: *Climate Change 2013: The Physical Science Basis. Contribution of Working Group I to the Fifth Assessment Report of the Intergovernmental Panel on Climate Change* [Stocker, T.F., Qin D., Plattner, G.-K., Tignor, M., Allen, S. K., Boschung, J., Nauels, A., Xia, Y., Bex, V. and Midgley, P. M. (Eds.)], Cambridge University Press, Cambridge, United Kingdom and New York, NY, USA, 2013.
- 675
- Burian, S. J., and Shepherd, J. M.: Effect of urbanization on the diurnal rainfall pattern in Houston, *Hydrol. Process.*, 19(5), 1089–1103, 2005.
- CARB: ARB’s Emission Inventory Activities, available at <https://www.arb.ca.gov/ei/ei.htm>, 2017.
- 680 Carnahan, W. H., and Larson, R. C.: An analysis of an urban heat sink, *Remote Sens. Environ.*, 33(1), 65–71, 1990.
- Carter, W. P. L.: The SAPRC-99 Chemical Mechanism and Updated VOC Reactivity Scales, available at: <http://www.engr.ucr.edu/~carter/reactdat.htm>, 2003.
- 685 Charlson, R. J., Schewartz, S. E., Hales, J. M., Cess, R. D., Coarley J. A., J., Hansen, J. E., and Hofmann, D. J.: Climate Forcing by Anthropogenic Aerosols, *Science*, 255(5043), 423–430, 1992.
- Chen, F., Dudhia, J.: Coupling an Advanced Land Surface–Hydrology Model with the Penn State–NCAR MM5 Modeling System. Part I: Model Implementation and Sensitivity, *Mon. Weather Rev.*, 129(4), 569–585, 2001.
- 690 Chen, F., Kusaka, H., Bornstein, R., Ching, J., Grimmond, C. S. B., Grossman-Clarke, S., Loridan, T., Manning, K. W., Martilli, A., Miao, S., Sailor, D., Salamanca, F. P., Taha, H., Tewari, M., Wang, X., Wyszogrodzki, A. A., Zhang, C.: The integrated WRF/urban modelling system: development, evaluation, and applications to urban environmental problems, *Int. J. Climatol.*, 31(2), 273–288, 2011.
- 695 Chen, L., Zhang, M., Zhu, J., Wang, Y., and Skorokhod, A.: Modeling Impacts of Urbanization and Urban Heat Island Mitigation on Boundary Layer Meteorology and Air Quality in Beijing Under Different Weather Conditions, *J. Geophys. Res.-Atmos.*, 123(8), 4323–4344, 2018.
- Ching, J., Brown, M., McPherson, T., Burian, S., Chen, F., Cionco, R., Hanna, A., Hultgren, T., McPherson, T., Sailor, D., Taha, H. and Williams, D.: National Urban Database and Access Portal Tool, *B. Am. Meteorol. Soc.*, 90(8), 1157–1168, 2009.

- 700 Chou, M.-D., and Suarez, M. J.: Technical Report Series on Global Modeling and Data Assimilation, Volume 15 - A Solar Radiation Parameterization for Atmospheric Studies, Goddard Space Flight Center, Greenbelt, MD, USA, 1999.
- Civerolo, K., Hogrefe, C., Lynn, B., Rosenthal, J., Ku, J.-Y., Solecki, W., Cox, J., Small, C., Rosenzweig, C., Goldberg, R., Knowlton, K. and Kinney, P.: Estimating the Effects of Increased  
705 Urbanization on Surface Meteorology and Ozone Concentrations in the New York City Metropolitan Region, *Atmos. Environ.*, 41(9), 1803–1818, 2007.
- Dyer, A. J. and Hicks, B. B.: Flux-gradient Relationships in the Constant Flux Layer, *Q. J. Meteor. Soc.*, 96(410), 715–721, 1970.
- Epstein, S. A., Lee, S.-M., Katzenstein, A. S., Carreras-Sospedra, M., Zhang, X., Farina, S. C., Vahmani,  
710 P., Fine, P. M., Ban-Weiss, G.: Air-quality Implications of Widespread Adoption of Cool Roofs on Ozone and Particulate Matter in Southern California, *P. Natl. Acad. Sci. USA*, 114(34), 8991–8996, 2017.
- Fallmann, J., Forkel, R. and Emeis, S.: Secondary Effects of Urban Heat Island Mitigation Measures on Air Quality, *Atmos. Environ.*, 125, 199–211, 2016.
- 715 Fan, C., Myint, S., Kaplan, S., Middel, A., Zheng, B., Rahman, A., Huang, H.-P., Brazel, A. and Blumberg, D. G.: Understanding the Impact of Urbanization on Surface Urban Heat Islands—A Longitudinal Analysis of the Oasis Effect in Subtropical Desert Cities, *Remote Sens.*, 9(7), 672, 2017.
- Fry, J., Xian, G. Z., Jin, S., Dewitz, J., Homer, C. G., Yang, L., Barnes, C. A., Herold, N. D. and  
720 Wickham, J. D.: Completion of the 2006 National Land Cover Database for the Conterminous United States, *Photogramm. Eng. Rem. S.*, 77(9), 858–864, 2011.
- Garratt, J. R.: The Atmospheric Boundary Layer [Houghton, J. T., Rycroft, M. J., and Dessler, A. J. (Eds.)], Cambridge University Press, Cambridge, United Kingdom, 1994.
- Georgescu, M., Morefield, P. E., Bierwagen, B. G., and Weaver, C. P.: Urban Adaptation can Roll Back  
725 Warming of Emerging Megapolitan Regions, *P. Natl. Acad. Sci. USA*, 111(8), 2909–14, 2014.
- Grell, G. A., and Dévényi, D.: A Generalized Approach to Parameterizing Convection Combining Ensemble and Data Assimilation Techniques, *Geophys. Res. Lett.*, 29(14), 38-1-38–4, 2012.
- Grell, G. A., Peckham, S. E., Schmitz, R., McKeen, S. A., Frost, G., Skamarock, W. C. and Eder, B.: Fully Coupled “Online” Chemistry within the WRF Model, *Atmos. Environ.*, 39(37), 6957–6975,

- 730 2005.
- Grimm, N. B., Faeth, S. H., Golubiewski, N. E., Redman, C. L., Wu, J., Bai, X. and Briggs, J. M.: Global Change and the Ecology of Cities, *Science*, 319(5864), 756–60, 2008.
- Guenther, A., Karl, T., Harley, P., Wiedinmyer, C., Palmer, P. I. and Geron, C.: Estimates of Global Terrestrial Isoprene Emissions using MEGAN (Model of Emissions of Gases and Aerosols from Nature), *Atmos. Chem. Phys.*, 6, 3181–3210, 2006.
- 735 Hardin, A. W. and Vanos, J. K.: The Influence of Surface Type on the Absorbed Radiation by a Human Under Hot, Dry Conditions. *Int. J. Biometeorol.*, 62(1), 43–56, 2018.
- Hassan, S. K., El–Abssawy, A. A. and Khoder, M. I.: Characteristics of Gas–Phase Nitric Acid and Ammonium–Nitrate– Sulfate Aerosol, and Their Gas–Phase Precursors in a Suburban Area in Cairo, Egypt, *Atmos. Pollut. Res.*, 4(1), 117–129, 2013.
- 740 Hong, S.-Y., Noh, Y., Dudhia, J., Hong, S.-Y., Noh, Y. and Dudhia, J.: A New Vertical Diffusion Package with an Explicit Treatment of Entrainment Processes, *Mon. Weather Rev.*, 134(9), 2318–2341, 2016.
- Imhoff, M. L., Zhang, P., Wolfe, R. E. and Bounoua, L.: Remote Sensing of the Urban Heat Island Effect Across Biomes in the Continental USA, *Remote Sens. Environ.*, 114(3), 504–513, 2010.
- 745 Jiang, X., Wiedinmyer, C., Chen, F., Yang, Z.-L. and Lo, J. C.-F.: Predicted Impacts of Climate and Land Use Change on Surface Ozone in the Houston, Texas, Area, *J. Geophys. Res.*, 113(D20), D20312, 2008.
- Kalnay, E. and Cai, M. Impact of Urbanization and Land-Use Change on Climate, *Nature*, 423(6939), 528–531, 2003.
- 750 Kim, S.-W., Heckel, A., Frost, G. J., Richter, A., Gleason, J., Burrows, J. P., McKeen, S., Hsie, E.-Y., Granier, C. and Trainer, M.: NO<sub>2</sub> Columns in the Western United States Observed from Space and Simulated by a Regional Chemistry Model and Their Implications for NO<sub>x</sub> Emissions, *J. Geophys. Res.*, 114(D11), D11301, 2009.
- 755 Kumar, R., Mishra, V., Buzan, J., Kumar, R., Shindell, D. and Huber, M.: Dominant Control of Agriculture and Irrigation on Urban Heat Island in India, *Sci. Rep.-UK*, 7(1), 14054, 2017.
- Kusaka, H., Chen, F., Tewari, M., Dudhia, J., Gill, D. O., Duda, M. G., Wang, W. and MiyaI, Y.: Numerical Simulation of Urban Heat Island Effect by the WRF Model with 4-km Grid Increment: An Inter-Comparison Study between the Urban Canopy Model and Slab Model, *J. Meteorol. Soc.*

- 760 JPN. Ser. II, 90B(0), 33–45, 2012.
- Kusaka, H., Kondo, H., Kikegawa, Y. and Kimura, F.: A Simple Single-Layer Urban Canopy Model For Atmospheric Models: Comparison With Multi-Layer And Slab Models, *Bound.-Lay. Meteorol.*, 101(3), 329–358, 2001.
- Li, D. and Bou-Zeid, E.: Quality and Sensitivity of High-Resolution Numerical Simulation of Urban  
765 Heat Islands, *Environ. Res. Lett.*, 9(5), 055001, 2014.
- Li, M., Wang, T., Xie, M., Zhuang, B., Li, S., Han, Y., Song, Y. and Cheng, N.: Improved Meteorology and Ozone Air Quality Simulations Using MODIS Land Surface Parameters in the Yangtze River Delta Urban Cluster, China, *J. Geophys. Res.-Atmos.*, 122(5), 3116–3140, 2017.
- Lin, Y.-L., Farley, R. D., Orville, H. D., Lin, Y.-L., Farley, R. D. and Orville, H. D. Bulk  
770 Parameterization of the Snow Field in a Cloud Model. *J. Clim. Appl. Meteorol.*, 22(6), 1065–1092, 1983.
- Lippmann, M.: Health Effects of Ozone: A Critical Review, *JAPCA J. Air Waste Ma.*, 39(5), 672–695, 1989.
- Madronich, S.: Photodissociation in the Atmosphere: 1. Actinic Flux and the Effects of Ground  
775 Reflections and Clouds. *J. Geophys. Res.*, 92(D8), 9740, 1987.
- Marr, L. C. and Harley, R. A.: Spectral Analysis of Weekday–Weekend Differences in Ambient Ozone, Nitrogen Oxide, and Non-Methane Hydrocarbon Time Series in California. *Atmos. Environ.*, 36, 2327–2335, 2002.
- Mesinger, F., DiMego, G., Kalnay, E., Mitchell, K., Shafran, P. C., Ebisuzaki, W., Jović, D., Woolen, J.,  
780 Rogers, E., Berbery, E. H., Ek, M. B., Fan, Y., Grumbine, R., Higgins, W., Li, H., Lin, Y., Manikin, G., Parrish, D. and Shi, W.: North American Regional Reanalysis, *B. Am. Meteorol. Soc.*, 87(3), 343–360, 2006.
- Mlawer, E. J., Taubman, S. J., Brown, P. D., Iacono, M. J. and Clough, S. A.: Radiative Transfer for Inhomogeneous Atmospheres: RRTM, a Validated Correlated-k Model for the Longwave. *J.*  
785 *Geophys. Res.-Atmos.*, 102(D14), 16663–16682, 1997
- Oke, T. R.: The Energetic Basis of the Urban Heat Island, *Q. J. Roy. Meteorol. Soc.*, 108(455), 1–24, 1982.
- Pankow, J. F.: Partitioning of Semi-Volatile Organic Compounds to the Air/Water Interface. *Atmos. Environ.*, 31(6), 927–929, 1997.

- 790 Paulson, C. A.: The Mathematical Representation of Wind Speed and Temperature Profiles in the Unstable Atmospheric Surface Layer, *J. Appl. Meteorol.*, 9(6), 857–861, 1970.
- Peng, S., Piao, S., Ciais, P., Friedlingstein, P., Oettle, C., Breón, F. O.-M. Nan, H., Zhou, L. and Myneni, R. B.: Surface Urban Heat Island Across 419 Global Big Cities. *Environ. Sci. Technol.*, 46, 696–703, 2012.
- 795 Pope, C. A. and Dockery, D. W.: Health Effects of Fine Particulate Air Pollution: Lines that Connect, *J. Air Waste Ma.*, 56(6), 709–742, 2006.
- Qiao, Z., Tian, G. and Xiao, L.: Diurnal and Seasonal Impacts of Urbanization on the Urban Thermal Environment: A Case Study of Beijing Using MODIS Data, *ISPRS J. Photogramm.*, 85, 93–101, 2013.
- 800 Rao, S. T., Ku, J. Y., Berman, S., Zhang, K. and Mao, H.: Summertime Characteristics of the Atmospheric Boundary Layer and Relationships to Ozone Levels over the Eastern United States, *Pure Appl. Geophys*, 160(1–2), 21–55, 2003.
- Rizwan, A. M., Dennis, L. Y. C. and Liu, C.: A Review on the Generation, Determination and Mitigation of Urban Heat Island, *J. Environ. Sci.*, 20(1), 120–128, 2008.
- 805 SCAQMD: Final 2016 Air Quality Management Plan, Appendix III: Base and Future Year Emission Inventory, available at: <http://www.aqmd.gov/docs/default-source/clean-air-plans/air-quality-management-plans/2016-air-quality-management-plan/final-2016-aqmp/appendix-iii.pdf>, 2017.
- Seto, K. C., Güneralp, B. and Hutyrá, L. R.: Global Forecasts of Urban Expansion to 2030 and Direct  
810 Impacts on Biodiversity and Carbon Pools, *P. Natl. Acad. Sci. USA*, 109(40), 16083–8, 2012.
- Steiner, A. L., Davis, A. J., Sillman, S., Owen, R. C., Michalak, A. M. and Fiore, A. M. Observed Suppression of Ozone Formation at Extremely High Temperatures due to Chemical and Biophysical Feedbacks, *P. Natl. Acad. Sci. USA*, 107(46), 19685–90, 2010.
- Stewart, I. D. and Oke, T. R.: Local Climate Zones for Urban Temperature Studies, *B. Am. Meteorol.*  
815 *Soc.*, 93(12), 1879–1900, 2012.
- Stockwell, W. R., Kirchner, F., Kuhn, M. and Seefeld, S.: A New Mechanism for Regional Atmospheric Chemistry Modeling, *J. Geophys. Res.-Atmos.*, 102(D22), 25847–25879, 1997.
- Stockwell, W. R., Middleton, P., Chang, J. S. and Tang, X.: The Second Generation Regional Acid Deposition Model Chemical Mechanism for Regional Air Quality Modeling, *J. Geophys. Res.*,

- 820 95(D10), 16343, 1990.
- Taha, H.: Meteorological, Air-Quality, and Emission-Equivalence Impacts of Urban Heat Island Control in California, *Sustain. Cities Soc.*, 19, 207–221, 2015.
- Tao, W., Liu, J., Ban-Weiss, G. A., Hauglustaine, D. A., Zhang, L., Zhang, Q., Cheng, Y., Yu, Y. and  
825 Tao, S.: Effects of Urban Land Expansion on the Regional Meteorology and Air Quality of Eastern China, *Atmos. Chem. Phys.*, 15(15), 8597–8614, 2015.
- Theeuwes, N. E., Steeneveld, G.-J., Ronda, R. J., Rotach, M. W. and Holtslag, A. A. M.: Cool City Mornings by Urban Heat, *Environ. Res. Lett.*, 10(11), 114022, 2015.
- U.S. EPA.: Profile of the 2011 National Air Emissions Inventory, available at: [https://www.epa.gov/sites/production/files/2015-08/documents/lite\\_finalversion\\_ver10.pdf](https://www.epa.gov/sites/production/files/2015-08/documents/lite_finalversion_ver10.pdf), 2014.
- 830 Vahmani, P. and Ban-Weiss, G. A.: Impact of Remotely Sensed Albedo and Vegetation Fraction on Simulation of Urban Climate in WRF-Urban Canopy Model: A Case Study of the Urban Heat Island in Los Angeles, *J. Geophys. Res.-Atmos.*, 121(4), 1511–1531, 2016a.
- Vahmani, P. and Ban-Weiss, G.: Climatic Consequences of Adopting Drought-Tolerant Vegetation Over Los Angeles as a Response to California Drought, *Geophys. Res. Lett.*, 43(15), 8240–8249,  
835 2016b.
- Vahmani, P. and Hogue, T. S.: Incorporating an Urban Irrigation Module into the Noah Land Surface Model Coupled with an Urban Canopy Model, *J. Hydrometeorol.*, 15(4), 1440–1456, 2014.
- Vahmani, P., Sun, F., Hall, A. and Ban-Weiss, G.: Investigating the Climate Impacts of Urbanization and the Potential for Cool Roofs to Counter Future Climate Change in Southern California,  
840 *Environ. Res. Lett.*, 11(12), 124027, 2016.
- Wang, K., Jiang, S., Wang, J., Zhou, C., Wang, X. and Lee, X.: Comparing the Diurnal and Seasonal Variabilities of Atmospheric and Surface Urban Heat Islands Based on the Beijing Urban Meteorological Network, *J. Geophys. Res.-Atmos.*, 122(4), 2131–2154, 2017.
- Wesely, M. L.: Parameterization of Surface Resistances to Gaseous Dry Deposition in Regional-Scale  
845 Numerical Models, *Atmos. Environ.* (1967), 23(6), 1293–1304, 1989.
- Wickham, J. D., Stehman, S. V., Gass, L., Dewitz, J., Fry, J. A. and Wade, T. G.: Accuracy Assessment of NLCD 2006 Land Cover and Impervious Surface, *Remote Sens. Environ.*, 130, 294–304, 2013.
- Xu, M., Chang, C.-P., Fu, C., Qi, Y., Robock, A., Robinson, D. and Zhang, H.: Steady Decline of East

Asian Monsoon Winds, 1969–2000: Evidence from Direct Ground Measurements of Wind Speed,  
850 J. Geophys. Res., 111(D24), D24111, 2006.

Yang, J., Wang, Z.-H., Chen, F., Miao, S., Tewari, M., Voogt, J. A. and Myint, S.: Enhancing  
Hydrologic Modelling in the Coupled Weather Research and Forecasting–Urban Modelling  
System, Bound.-Lay. Meteorol., 155(1), 87–109, 2015.

Zhang, J., Mohegh, A., Li, Y., Levinson, R., and Ban-Weiss, G.: Systematic Comparison of the  
855 Influence of Cool Wall Versus Cool Roof Adoption on Urban Climate in the Los Angeles Basin,  
Environ. Sci. Technol. (In press), 2018a.

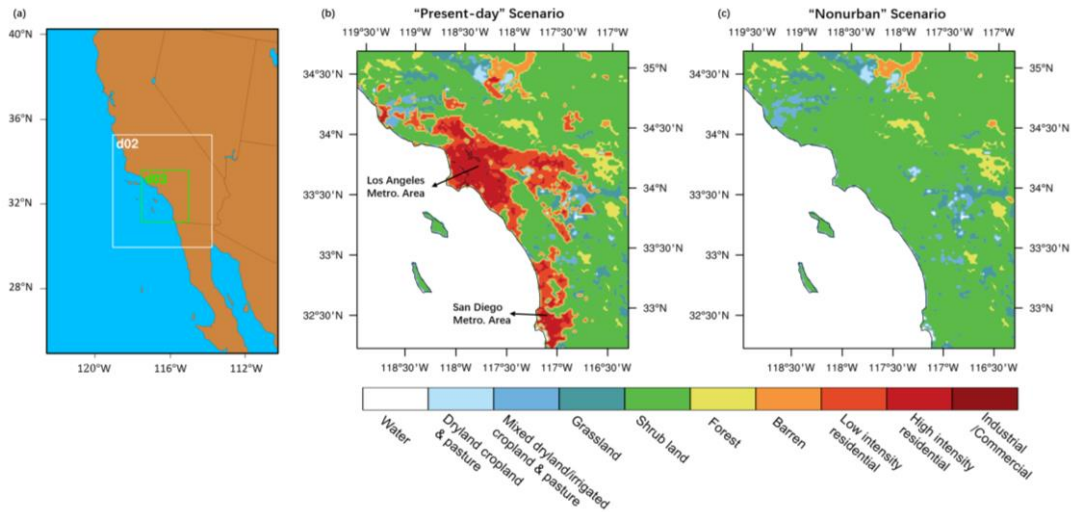
Zhang, J., Li, Y., Tao, W., Liu, J., Levinson, R., Mohegh, A. and Ban-Weiss., G.: Investigating the  
Urban Air Quality Effects of Cool Walls and Cool Roofs in Southern California, submitted to  
Environ. Sci. Technol., 2018b.

860 Zhang, N., Gao, Z., Wang, X. and Chen, Y.: Modeling the Impact of Urbanization on the Local and  
Regional Climate in Yangtze River Delta, China, Theor. Appl. Climatol., 102(3–4), 331–342,  
2010.

Zhao, L., Lee, X., Smith, R. B. and Oleson, K.: Strong Contributions of Local Background Climate to  
Urban Heat Islands, 511(7408), 216–219, 2014.

865

## Figures and Tables



870 | **Figure 1.** Maps of (a) the three nested ~~WRF/Chem~~WRF-UCM-~~Chem~~UCM domains, and (b,c) land cover types for the innermost domain (d03) for the (b) Present-day and (c) Nonurban scenarios.

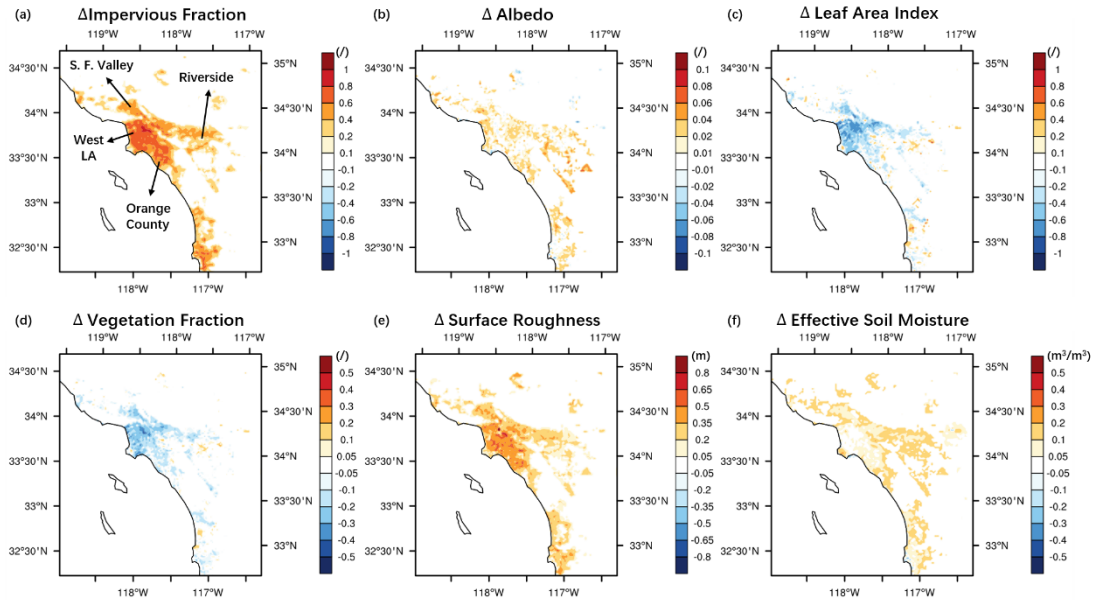


**Figure 2.** Spatial patterns of differences (Present-day – Nonurban) in land surface properties for urban grid cells. Panels (a) to (f) are changes in impervious fraction, albedo, leaf area index (LAI), vegetation fraction (VEGFRA), surface roughness, and effective soil moisture, respectively. Effective soil moisture is calculated as the product of pervious fraction for urban grid cells ( $1 - \text{impervious fraction}$ ) and soil moisture for the pervious portion of the grid cell.

875

880

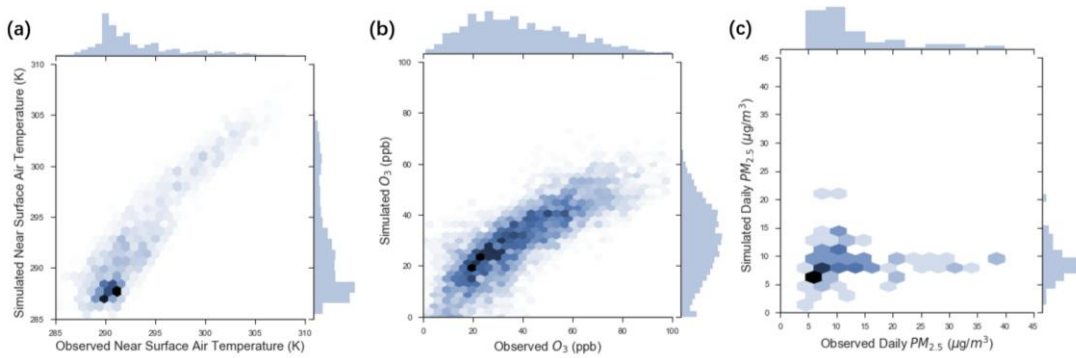


**Figure 3.** Comparison between modeled and observed (a) hourly near-surface air temperature (K), (b) hourly O<sub>3</sub> concentrations (ppb), and (c) daily PM<sub>2.5</sub> concentrations (µg/m<sup>3</sup>). Note that daily PM<sub>2.5</sub> concentrations from simulations include sea salt, but exclude dust. Darker hexagonal bins correspond to higher point densities in the scatter plots. Histograms of both observations and modeled values are also shown at the edges of each panel.

885

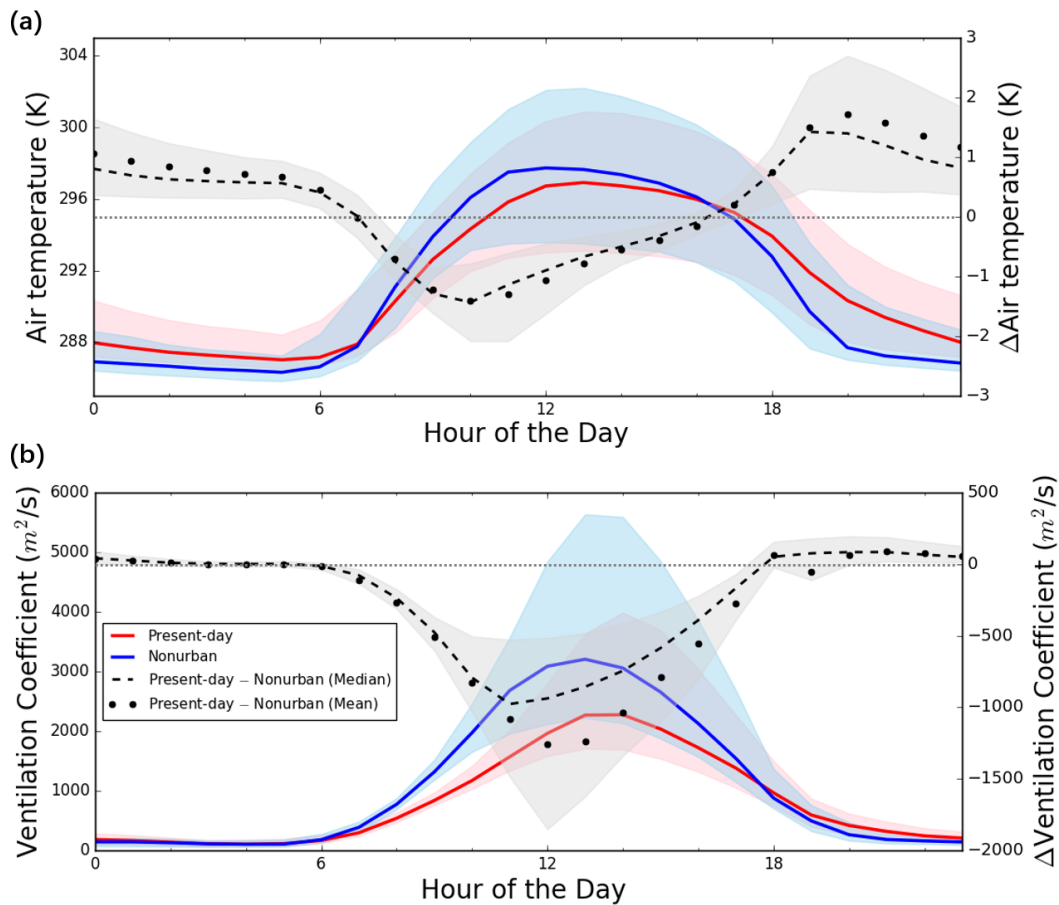
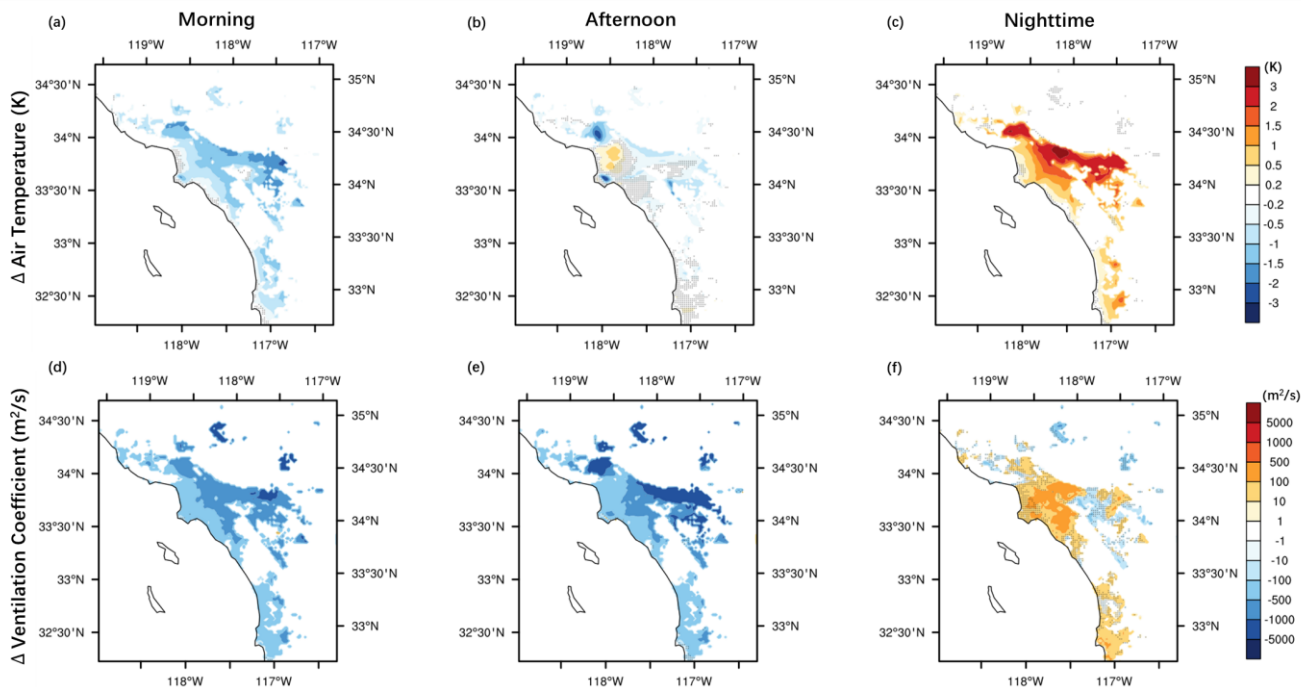


**Figure 4.** Diurnal cycles for present-day (red), nonurban (blue), and present-day – nonurban (black) for (a) air temperature in the lowest atmospheric layer (K) and (b) ventilation coefficient ( $m^2/s$ ). Values are obtained by averaging over urban grid cells and the entire simulation period for each hour of day. The solid and dashed curves give the median values, while the shaded bands show 25<sup>th</sup> and 75<sup>th</sup> percentiles. Dots indicate mean values for differences between Present-day and nonurban. The horizontal dotted line in light grey shows  $\Delta=0$  as an indicator of positive or negative change by land surface changes via urbanization.

890



895 **Figure 5.** Spatial patterns of differences (Present-day – nonurban) in temporally averaged values during morning, afternoon and nighttime for (a,b,c) air temperature in the lowest atmospheric layer, and (d,e,f) ventilation coefficient. Morning is defined as 7 PST to 12 PST, afternoon as 12 PST to 19 PST, and nighttime as 19 PST to 7 PST. We refer to morning and afternoon as daytime. Note that values are shown only for urban grid cells. Black dots indicate grid cells where changes are not significantly different from zero at 95% confidence level using the paired Student’s t-test with  
 900  $n=7$  days.

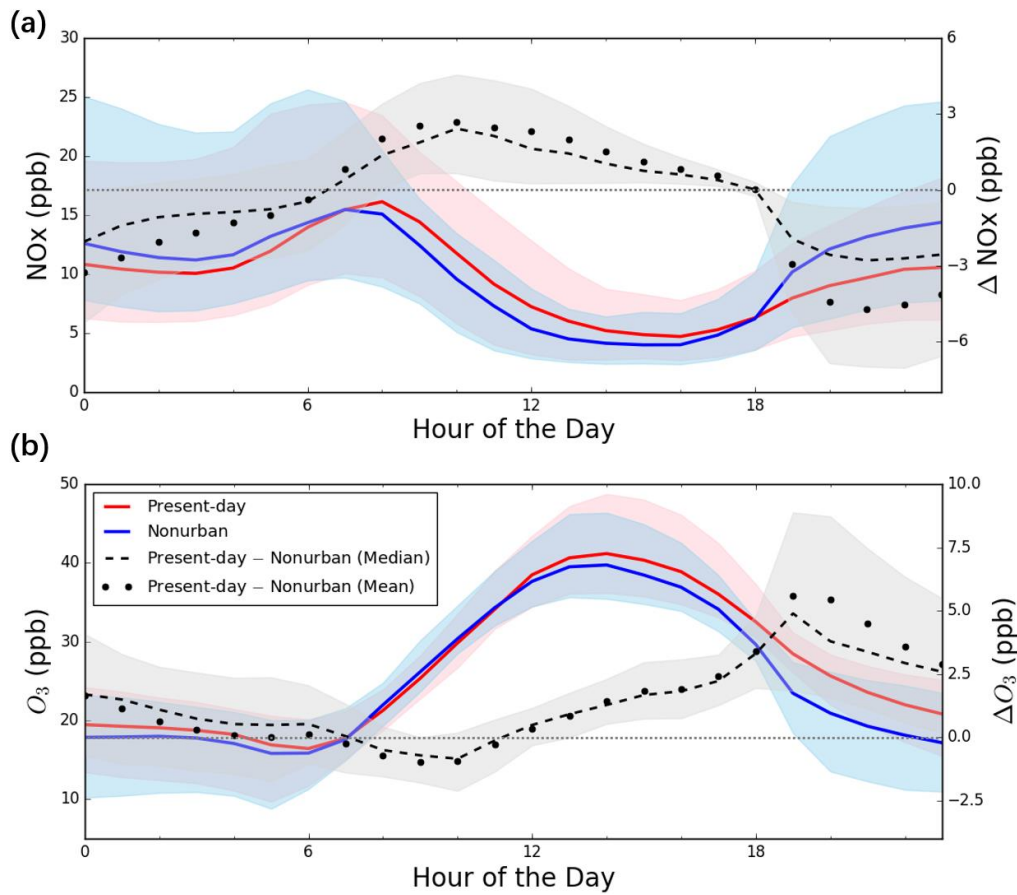
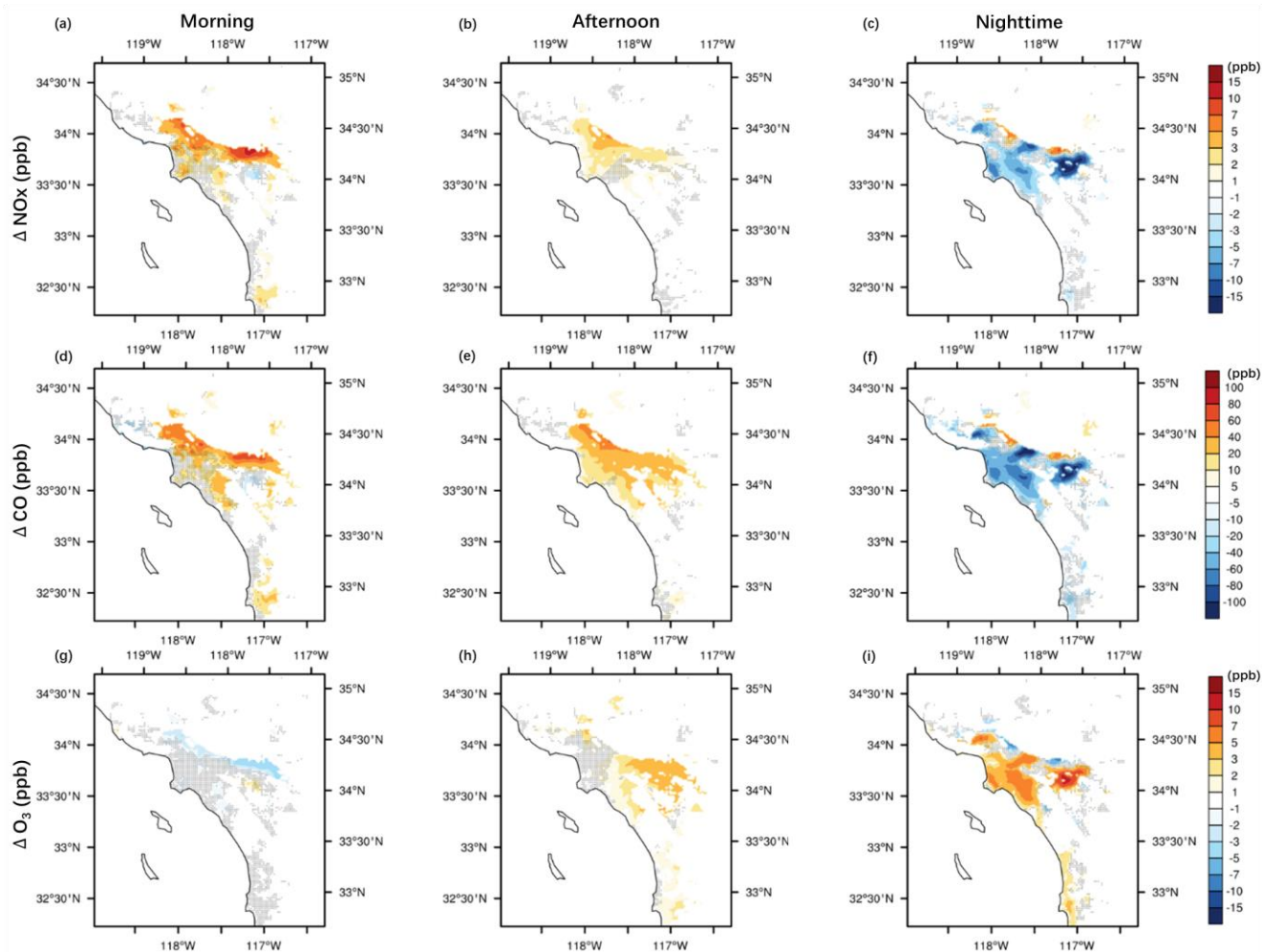


**Figure 6.** Diurnal cycles for present-day (red), nonurban (blue), and present-day – nonurban (black) for (a) NO<sub>x</sub> (ppb) and (b) O<sub>3</sub> concentrations (ppb). Values are obtained by averaging over urban grid cells and the entire simulation period for each hour of day. The solid and dashed curves give the median values, while the shaded bands show 25<sup>th</sup> and 75<sup>th</sup> percentiles. Dots indicate mean values for differences between Present-day and nonurban. The horizontal dotted line in light gray shows  $\Delta = 0$  as an indicator of positive or negative change by land surface changes via urbanization.

905



910

**Figure 7.** Spatial patterns in differences (Present-day – nonurban) of temporally averaged values during morning, afternoon and nighttime for (a,b,c) NO<sub>x</sub>, (d,e,f) CO, and (g,h,i) O<sub>3</sub> concentrations. Morning is defined as 7 PST to 12 PST, afternoon as 12 PST to 19 PST, and nighttime as 19 PST to 7 PST. Black dots indicate grid cells where changes are not significantly different from zero at 95% confidence level using the paired Student's t-test with n=7 days.

915

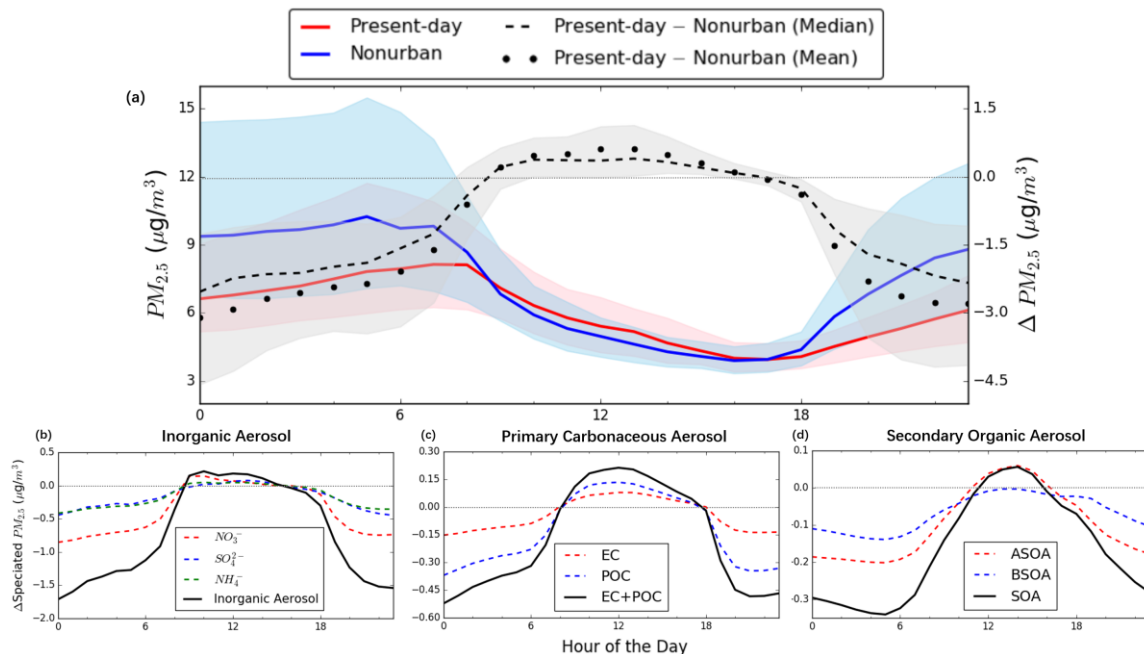


**Figure 8.** Diurnal cycles for spatially averaged PM<sub>2.5</sub> concentrations. Panel (a) shows Present-day, nonurban, and present-day – nonurban for total PM<sub>2.5</sub> (excluding sea salt and dust). The lower row shows differences (Present-day – nonurban) in speciated PM<sub>2.5</sub> including (b) inorganic aerosols (NO<sub>3</sub><sup>-</sup>, SO<sub>4</sub><sup>2-</sup>, NH<sub>4</sub><sup>+</sup>), (c) primary carbonaceous aerosols (EC, POC), and (d) secondary organic aerosols (ASOA, BSOA). The horizontal dotted line in light grey is shown for Δ = 0 as an indicator of positive or negative change by urbanization.

920

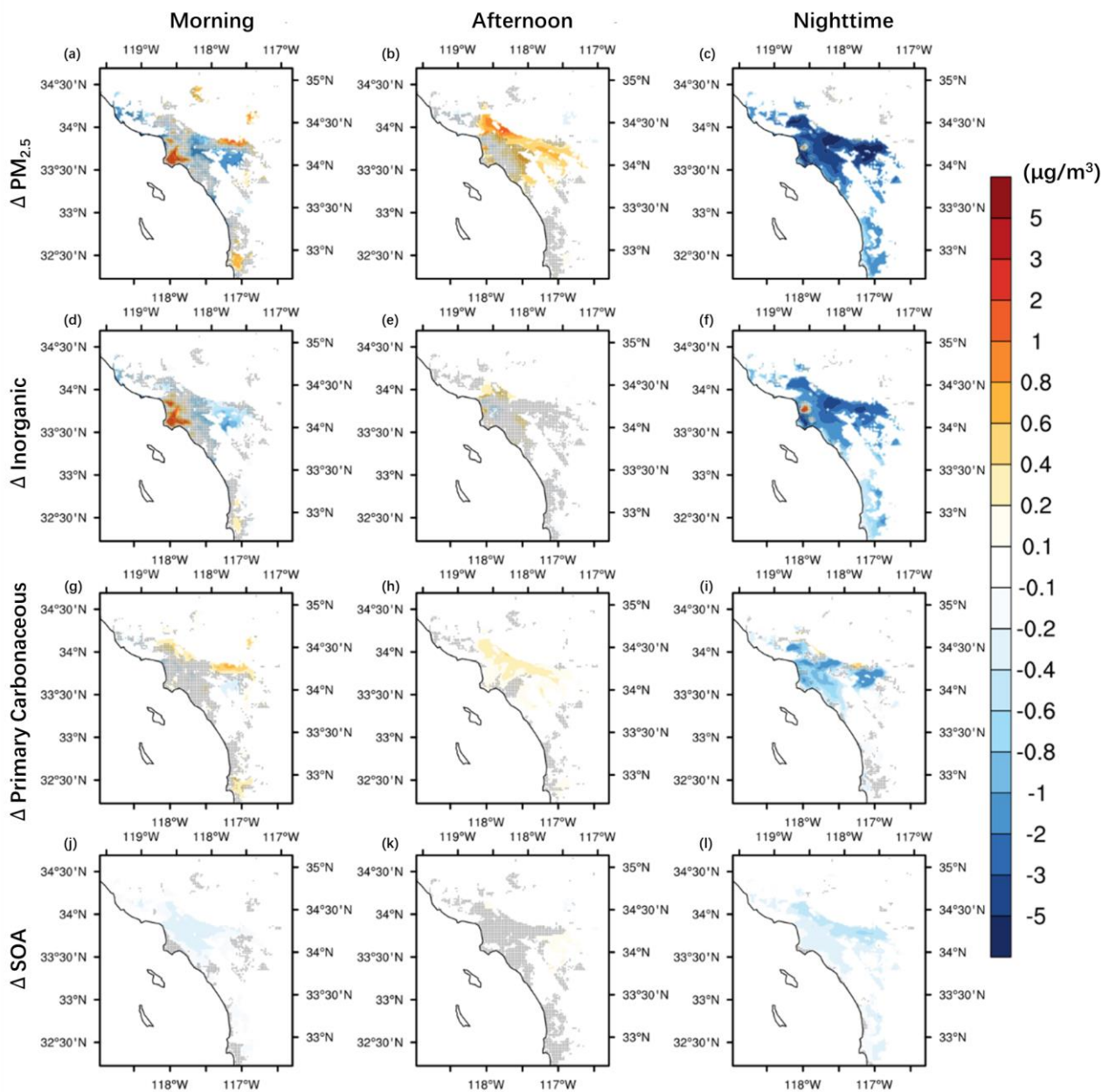


**Figure 9.** Spatial patterns in differences (Present-day – nonurban) of temporally averaged values during morning, afternoon, and nighttime for  $PM_{2.5}$ . Panels (a)–(c) show total  $PM_{2.5}$ ; (d)–(f) inorganic aerosol; (g)–(i) primary carbonaceous aerosol; and (j)–(l) secondary organic aerosol. Morning is defined as 7 PST to 12 PST, afternoon as 12 PST to 19 PST, and nighttime as 19 PST to 7 PST. Black dots indicate grid cells where changes are not significantly different from zero at 95% confidence level using the paired Student's t-test with  $n=7$  days.

930 Table 1. Summary statistics (mean bias (MB), normalized mean bias (NMB), mean error (ME), and root mean square error (RMSE)) for model evaluation, which compares simulated hourly near-surface air temperature (T2), hourly O<sub>3</sub> and daily PM<sub>2.5</sub> concentrations to observations.

Variable	N <sup>a</sup>	Mean		MB <sup>b</sup>	NMB <sup>c</sup>	ME <sup>d</sup>	RMSE <sup>e</sup>
		Observations	Simulations				
T2	1944	293.0 K	292.0 K	-1.0 K	-0.3%	1.9 K	2.2 K
O <sub>3</sub>	5171	38.7 ppb	30.0 ppb	-8.7 ppb	-22%	11.8 ppb	14.6 ppb
PM <sub>2.5</sub>	81	12.9 µg/m <sup>3</sup>	9.2 µg/m <sup>3</sup>	-4.0 µg/m <sup>3</sup>	-31%	6.2 µg/m <sup>3</sup>	9.5 µg/m <sup>3</sup>

<sup>a</sup>. Total number of data points comparing modeled versus observed values across all measurement station locations over the simulation period

$$\text{b. MB} = \frac{1}{N} \sum (mol_i - obs_i)$$

$$\text{c. NMB} = \frac{\sum (mol_i - obs_i)}{\sum obs_i}$$

$$\text{d. ME} = \frac{1}{N} \sum |mol_i - obs_i|$$

$$\text{e. RMSE} = \left[ \frac{1}{N} \sum (mol_i - obs_i)^2 \right]^{\frac{1}{2}}$$